THE RADIOACTIVE DECAY OF IRIDIUM-192

Thesis by

Leo L. Baggerly

In Partial Fulfillment of the Requirements

for the degree of

Doctor of Philosophy

California Institute of Technology

Pasadena, California

1956

The author wishes to express his thanks to the personnel of the research groups known as Physics 15 and Physics 34, all of whom have aided in some way in the production of this thesis. In particular, the assistance of Eastman Hatch and Sam Raff in the compilation of data is appreciated.

The inspiration and understanding shown by Dr. Jesse W. M. DuMond at several crucial periods is gratefully acknowledged.

The patient advice of Drs. Felix Boehm and Pierre Marmier has been of inestimable aid, and is deeply appreciated.

The work was supported by the Atomic Energy Commission.

Abstract

A study has been made of the gamma radiation following the decay of Ir^{192}. The energies, internal conversion coefficients and multipolarities of the gamma transitions have been determined. Energy level schemes for the daughter nuclei, Pt^{192} and Os^{192}, are proposed. The spins and parities of most of the levels are given. Some of the regularities found in heavy even-even nuclei have been confirmed for this decay.

Table of Contents

I. Summary

The dual decay of Ir^{192} to Pt^{192} and Os^{192} has been studied. The experimental apparatus included a precision curved crystal diffraction gamma spectrometer, a high-resolution beta spectrometer, and scintillation spectrometers. Gamma-gamma coincidence and angular correlation studies were carried out with the latter.

The energies of seventeen gamma rays, following the decay of Ir^{192}, have been measured. Of these, eleven have been assigned to transitions in Pt^{192}, and six to transitions in Os^{192}. The multipolarities of fourteen of the gamma rays were determined from their internal conversion coefficients. The transitions were all E2 or E2 + M1. (Table I.)

Ninety-six per cent of the decays of Ir^{192} proceed by beta emission to Pt^{192}. An energy level scheme has been proposed for the Pt^{192} branch of the decay. It includes seven energy levels at 316.5, 612.4, 784.5, 920.9, 1155, 1201 and 1359 kev. The spins of four of the levels, 316.5, 612.4, 784.5 and 1201 kev, have been determined to be 2, 2, 4 and 4, respectively. The spins of two other levels (920.9 and 1359) have been limited to one of two possibilities (3 or 4, in both cases). The parities of the above six levels are all even.

The endpoint energy of the most energetic beta group is 673 ± 10 kev. It apparently feeds the 784.5 kev level in Pt^{192}, indicating an Ir^{192} - Pt^{192} mass difference of 1457 ± 10 kev. Indirect evidence was found for three other beta groups, with endpoint energies of 536 ± 10, 256 ± 10, and 99 ± 12 kev. The four beta groups have relative intensities 48:41:7:$<$0.5. All are first forbidden transitions, having log ft values of 8.1 to 8.3.

Electron capture transitions make up 4% of the Ir^{192} decays. Three

alternative energy level schemes have been proposed for the Os^{192} branch. All involve four excited levels, at energies: 1) 205.7, 407.0, 690.4 and 1065 kev; 2) 205.7, 489.1, 690.4 and 1065 kev; or 3) 201.3, 484.7, 690.4 and 1065 kev. The spin assignments are the same for all three schemes. The spin of the first excited level is 2, that of the second is (1, 2 or 3), and the spin of the third excited state is (3 or 4). Parity of all three states is even.

Electron capture transitions feed the two levels at 690.4 and 1065 kev, in the ratio 2:1.5. Since no positrons were detected, an upper limit of 2.0 Mev can be placed on the Ir^{192} - Os^{192} mass difference. The spin and parity of the ground state of the Ir^{192} nucleus is (5 or 6)-.

Some of the regularities in energy, spins and relative intensities of transitions, which are found generally in the spectra of heavy even-even nuclei, have been observed in the decay of Ir^{192}. The energies of the first excited levels of Pt^{192} and Os^{192} fit well with those of the neighboring nuclei. The E_2/E_1 ratio in Pt^{192} is 1.94. The spins and parities of the first excited states are 2+ for both nuclei. The second level of Pt^{192} is also a 2+ state. The second-to-first excited state transitions are mostly E2, with relatively little M1 admixture. In Pt^{192}, the cross-over transition from the second level to the ground state is less intense than the second-to-first level transition, despite the higher energy of the former.

Generally, the energy level structure of Pt^{192} seems to be rather well settled. Remaining to be done are the removal of uncertainties in the spins of the 920.9 and 1359 kev levels, and the determination of the spin and parity of the 1155 kev level. While some progress has been made toward clarifying the Os^{192} branch of the decay, several problems remain to be solved.

II. Introduction

The considerable progress in nuclear spectroscopy in recent years is due in large part to the stimulating effect of two nuclear models, the shell model and the model of collective motions. These models have provided simple and natural explanations for many of the regularities found in nuclear spectroscopy. Of especial interest in this regard are the nuclei with high atomic weight, having an even number of protons and an even number of neutrons (the so-called even-even nuclei). Striking regularities have been found in their energy level structure, particularly as regards energies and spins of the first and second excited states.

One of the strong evidences of a nuclear shell structure, as predicted by the shell model, is found in the excitation energies of nuclei. It is observed that in those nuclei in which either a proton or a neutron shell is closed (Z or N = 50, 82, 126), the energy of the first excited state is relatively high. Examples of this are Ce^{140} (N = 82), in which the first excited level is at 1.6 Mev, and Pb^{208} (Z = 82, N = 126), in which it is at 2.6 Mev. (1) As can be seen in fig. 1, when the atomic number differs from 140 or 208, the energy of the first excited state decreases. (2)(3)(4)(5) It is lowest in the transuranic elements ($\sim$ 50 kev) and in the rare earth region ($\sim$ 100 kev).

The pattern of energy levels found in the rare earths and in the transuranic elements has been successfully interpreted on the basis of the model of collective motions, by Bohr and Mottelson. (6)(7)(8) The essential assumption of this model is that, far from a closed shell, the surface of the nucleus is deformed, or non-spherical. If the deformation has an axis of symmetry, the lowest modes of excitation are collective rotations about an axis perpendicular to the symmetry axis.

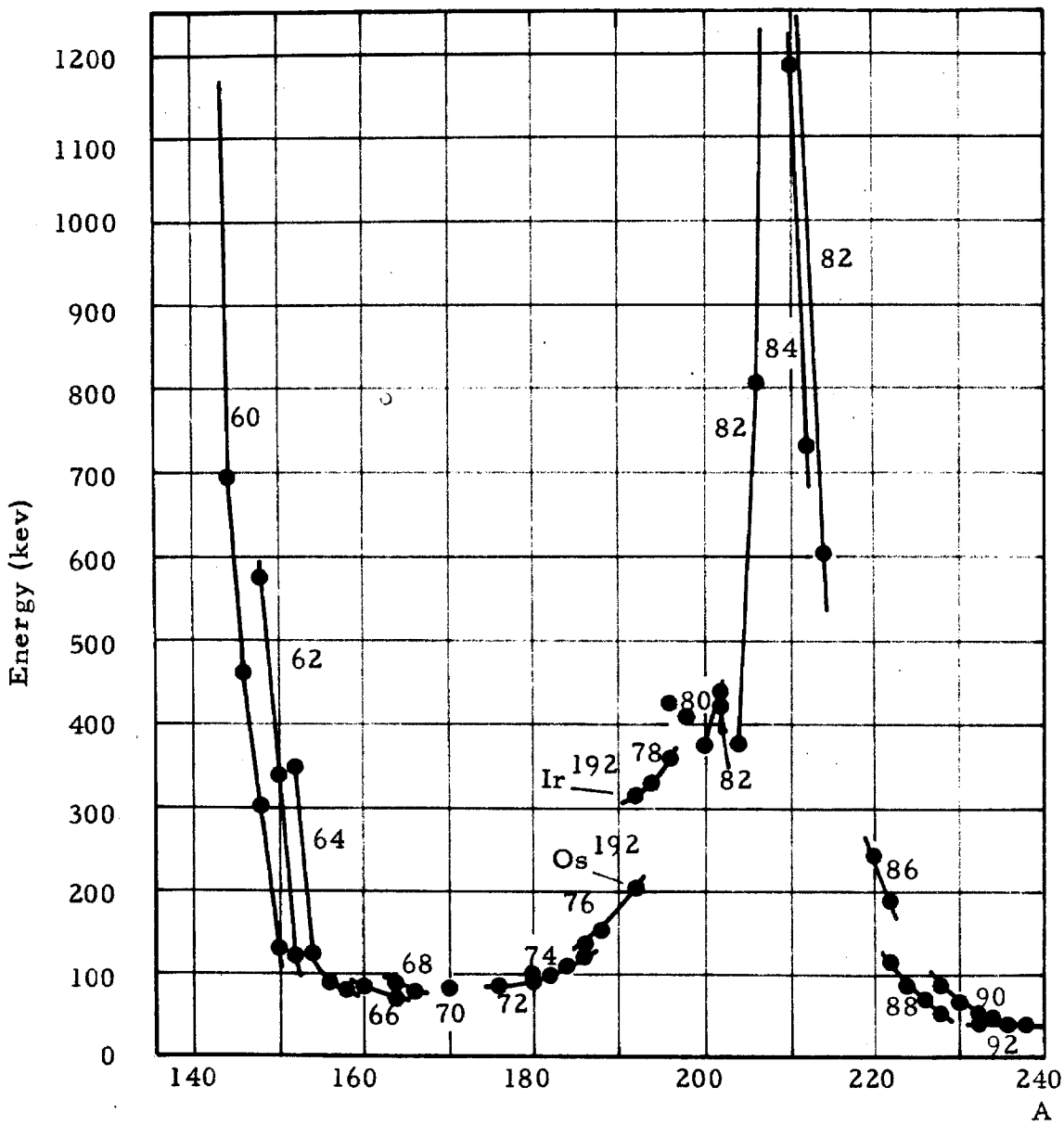

Fig. 1. Energy of the first excited states of even-even nuclei, as a function of mass number, A. ($140 \leq A \leq 240$) Lines connect isotopes of the same element. The numbers are the atomic numbers, Z, of the nuclei.

It is possible to show that the stationary states for such a collective rotation will have angular momenta $I/\hbar = 0, 2, 4, \ldots$, and even parity (for even-even nuclei). The energies of these allowed states will be

$$E = \frac{\hbar^2}{2J} I(I + 1)$$

where J is the moment of inertia for the collective motion, about the axis of rotation. This moment of inertia has been shown to be proportional to the square of a parameter describing the deformation. It will vanish for a spherically symmetric nucleus.

If we label the energy of the first, second, ..., excited states E_1, $E_2, \ldots$, then the energies of the rotational states are E_1, $E_2 = 10/3\, E_1$, $E_3 = 7\, E_1$, . . . The spins and parities of these states are 0+, 2+, 4+, . . . The levels are connected by cascading electric quadrupole transitions.

A survey of the experimental data (2)(3)(4) on the lowest two or three levels indeed reveals the predicted regularities. Figure 2 exhibits the E_2/E_1 ratio for those nuclei with $140 \leq A \leq 240$ for which data are available. As can be seen, in a number of the nuclei in the transuranic elements and in the rare earths, this ratio is very close to 10/3. In these same nuclei, the E_3/E_1 ratio, where it is known, is found to be close to 7.

As one approaches the closed shell configurations, the E_2/E_1 ratio drops from 10/3 to $\sim$2, indicating that the pattern of rotational states is being modified. There is evidence (e.g., from the electric quadrupole moments) that the deformation of nuclei in the neighborhood of closed shell configurations is very small. The transition from the pattern of the rotational levels, characteristic of the strongly deformed nuclei, to a different pattern is not abrupt, as can be seen from figs. 1 and 2. In addition to the increase in the excitation energy E_1 and a drop in the E_2/E_1 ratio as we approach the closed shell configuration, the sequence

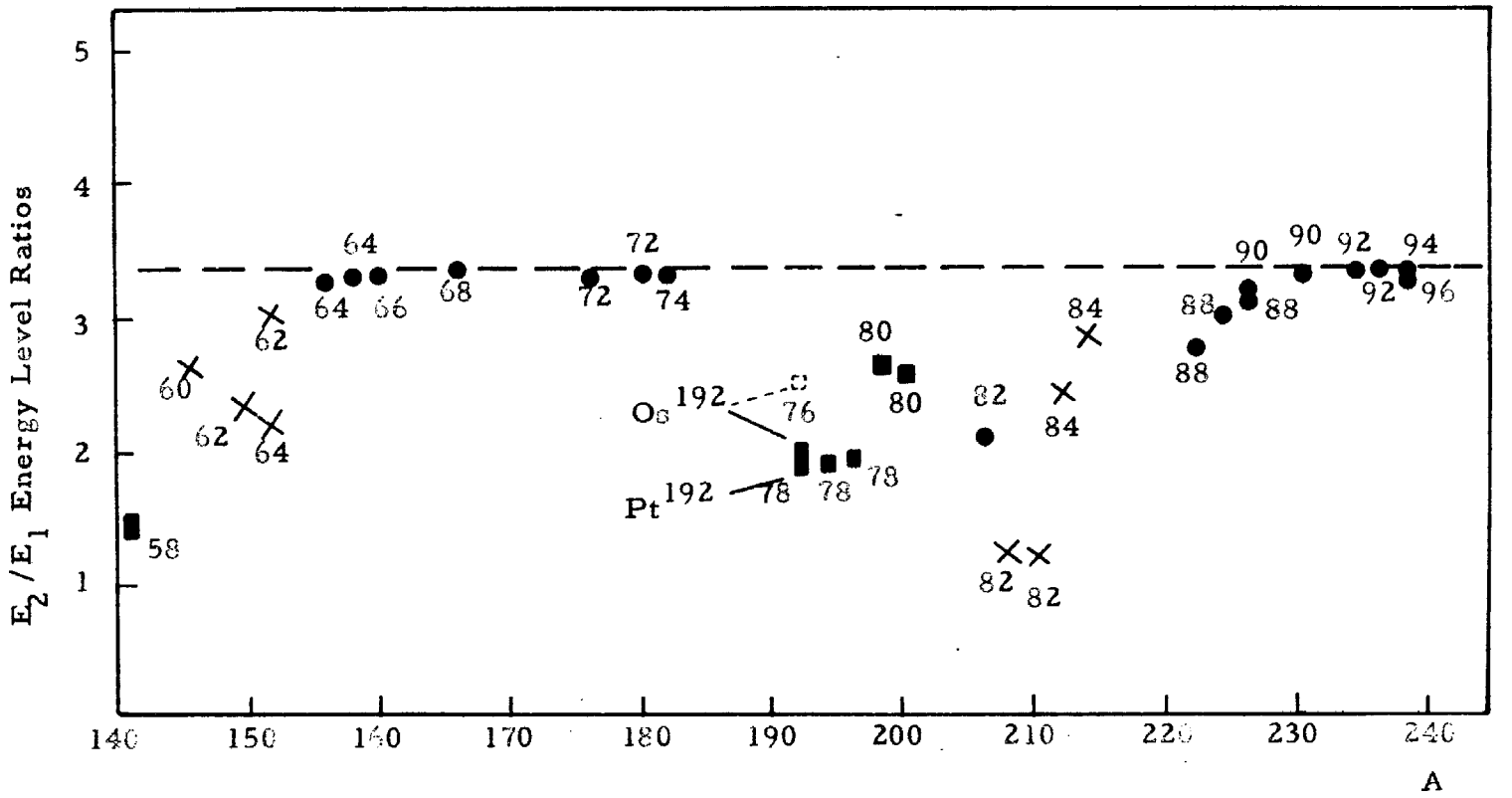

Fig. 2 Ratio of energies of second and first excited states, E_2/E_1, as a function of mass number A, ($140 \leq A \leq 240$). The spin and parity of the second excited state is denoted by ■ (2+), ● (4+), X (other, or unknown).

of spins of the first three levels appears to change from 0, 2, 4 to 0, 2, 2.

It is of interest, then, to investigate thoroughly a nucleus in this transition range. Ir^{192} is a good choice for such an investigation. It decays to Os^{192} by electron capture, and excites a number of levels in the Os^{192} nucleus. On the other hand, it also decays to Pt^{192} by beta emission, exciting several states in this nucleus. (8) This thesis is concerned with the study of this dual decay.

III. Apparatus

The instruments available, in this laboratory, for the study of nuclear spectra include a curved crystal diffraction gamma spectrometer, a beta spectrometer, and a coincidence system using scintillation counters. The interpretation of the final results, and the construction of a coherent decay scheme, depend on an intimate combination of the different kinds of information which each of these instruments provides. For example, the gamma spectrometer provides precision energy measurements of the gamma rays; gamma-gamma coincidences are measured with the scintillation counters; multipolarities of gamma rays can be deduced from ratios of the internal conversion coefficients measured by the beta spectrometer.

In this section, each of the instruments will be described, along with the corrections which are applied to the data provided by each one.

A. Gamma Spectrometer

i. General description

The gamma spectrometer was designed by DuMond, and its construction and operation have been described in detail by him, as well as by Lind. (9)(10)(11)(12) The principle of its operation can be easily understood with the aid of fig. 3. A crystal lamina, C, is bent so that its crystal planes, if extended, would intersect at a point, A. The "focal circle" is tangent to the neutral axis of the crystal at its center, and passes through point A. If a source of gamma rays is placed on the focal circle, at S, all the rays passing through the crystal intersect the crystal planes at very closely the same angle θ.

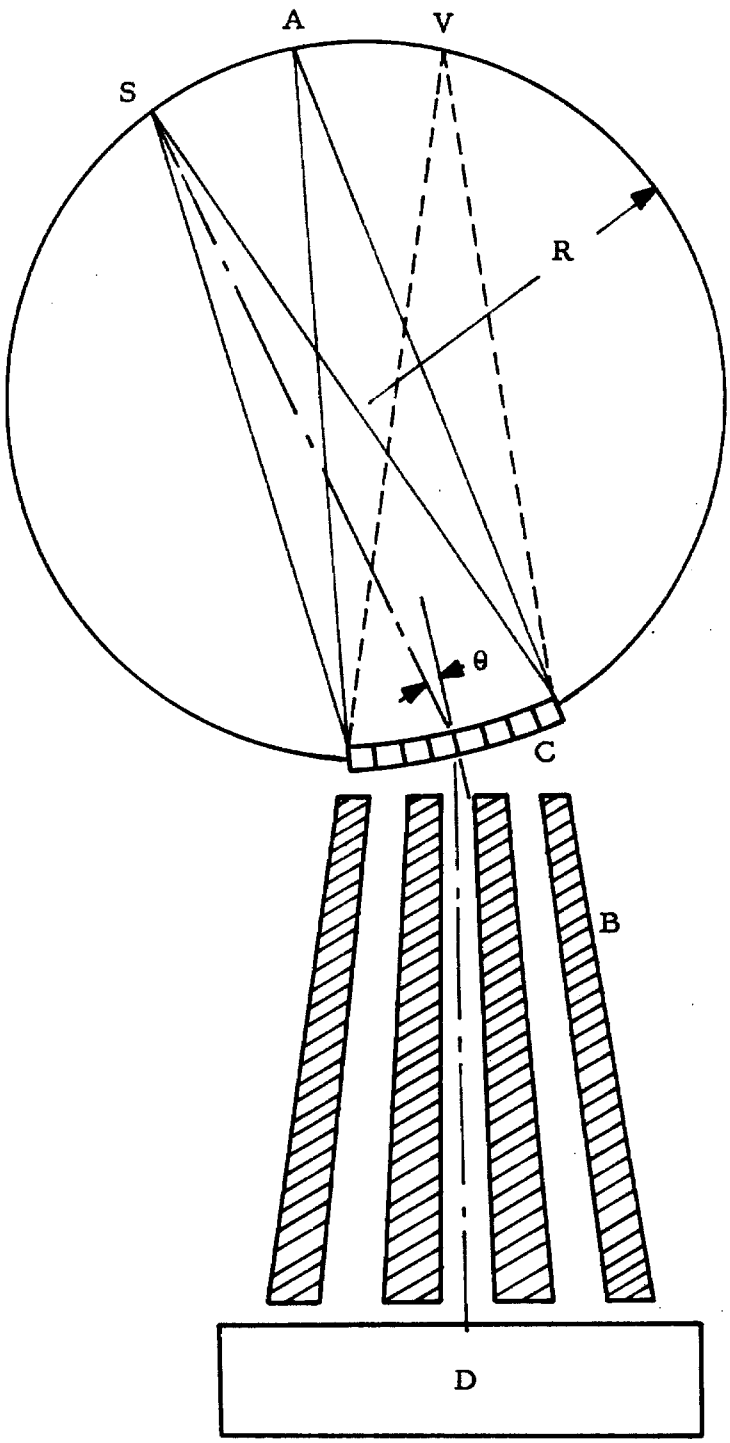

Fig. 3. Basic geometry of the curved crystal diffraction gamma spectrometer. S represents the source position; A, the axis of convergence of the crystal planes; V, the virtual focus; R, the radius of the focal circle; θ, the angle of incidence of gamma rays on the crystal planes; C, the curved crystal; B, the collimator; and D, the detector.

Constructive interference from the various planes occurs when θ coincides with the Bragg angle for the radiation - i.e., when $\lambda = 2 d \sin \theta$, for reflection in the first order. The reflected rays, making the same angle θ with the crystal planes, then diverge as if coming from the virtual focus at V. A collimator, B, which consists of a set of tapered lead sheets, positioned by tapered spacers, serves to separate the reflected beam from the much more intense direct beam. The detector, D, is placed behind the collimator.

In the spectrometer used, the radius of the focal circle is 1 meter. The bent crystal is a 2 mm thick slab of quartz, so cut that the 310 planes are normal to the faces. The detector is a cylindrical crystal of sodium iodide, 3 inches in diameter, and 2 inches thick. It is mounted on the face of a DuMont photomultiplier tube, which has a flat photocathode, 4 1/4 inches in diameter.

The pulses from the photomultiplier tube were fed to a linear amplifier, followed by a single channel differential discriminator. The output pulses from the discriminator were made uniform in height and length, and applied to a linear integrating circuit, the output of which is a D.C. voltage proportional to the counting rate. This voltage was applied to a Brown chart recorder. Alternatively, the pulses from the discriminator could be applied to a mechanical printer. At regular intervals, the printer would print the total number of counts accumulated in a preset counting interval, and, at the same time, would record the source position (i.e., the angle θ).

ii. Energy measurements

The gamma spectrometer is built so that it is symmetric about the diameter AC (fig. 3). Measurements can be made with the source on either side of this diameter, and thus with reflections from either side of the crystal planes. In terms of the diagram in fig. 3, the source position, S, and the virtual focus, V, can be interchanged. For a precision determination of the wavelength of a gamma line, measurements are made with source first on one side of A, and then on the other. The Bragg angle is taken as half the total angle between the two positions of the source.

The source is positioned by a precision positioning screw. Wavelengths are measured in the gamma spectrometer in units of revolutions of this positioning screw. The factors necessary to convert screw revolutions to milliangstroms have been thoroughly discussed by Muller (12), and will not be repeated here.

The width at half maximum of a simple line is about 0.25 mÅ, and is constant throughout the range of the instrument. Since $E\lambda$ = constant, and $d\lambda = dE/E^2$ = constant, the resolution expressed on an energy scale, $\Delta E/E$, is proportional to the energy, and is given by $\Delta E/E = 2 \cdot 10^{-5} E$, where E is given in kev. At 600 kev, this corresponds to an energy resolution of 1.25%.

The uncertainty assigned to the absolute values of the energies reported in this investigation is 1/20 of the resolution for distinct, well-separated lines. The reproducibility, and the internal consistency of the energies, is better than this by about a factor 2.

iii. Intensity measurements*

Intensities of gamma spectrometer lines must be corrected for:

1. absorption in the source and in the source container,

2. energy dependence of the sensitivity of the detector,

3. reflectivity of the bent quartz crystal.

The source has the shape of a rectangular parallelopiped (see part iv., Source preparation, gamma), which is oriented with one of its faces perpendicular to the direction of observation. It is easily shown that the ratio of the intensity, emitted perpendicular to one face, to that produced in the source is

$$\frac{I'}{I} = \frac{1}{\mu d}\left(1 - e^{-\mu d}\right)$$

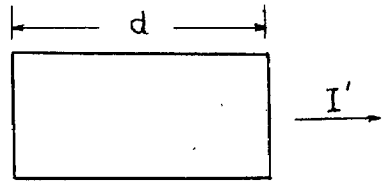

where μ is the absorption coefficient of the source material, and d is the dimension of the source in the direction of observation. The correction for the particular source being studied was small above 250 kev - below this it increased rapidly. At 85 kev, $I'/I = 0.01$. The source was aligned to within 3^{o}. A misalignment makes the most difference at low energies, where the absorption in the source is the greatest. If the source were misaligned by as much as 3^{o}, the maximum error in the correction for absorption in the source would be $\sim 25\%$ for the line of lowest energy measured (136 kev), and less than 10% for all others.

To measure the intensity of a line, the gamma spectrometer is first set on the peak of the line. Then the pulse height spectrum

---

* Intensity, as used throughout the following section, will mean relative intensity, unless specifically stated otherwise. No attempt was made to measure absolute intensities.

from the detector is recorded. (A typical spectrum is shown in fig. 6.) The total number of counts in the photopeak of the pulse height spectrum is then taken as the measure of the intensity of the line. This must be corrected for the photopeak efficiency of the detector. The method of determining the photopeak efficiency will be discussed in section III.C.

The proper correction to be applied for the reflectivity of the bent quartz crystal is somewhat uncertain at the present time. Marmier found some inconsistencies in the intensities of lines in Ta^{182} and Ta^{183} which had been measured with the gamma spectrometer, and has attributed them to an uncertainty in the crystal reflectivity. (13) This led to a re-examination of the work of Lind, (14), who had measured the integrated reflection coefficient of a curved quartz crystal as a function of wavelength. He found an energy dependence of about E^{-2}. Lind's measurements were made on a 1 mm thick crystal, whereas the crystal now in use is 2 mm thick, and the stresses introduced in the bending are correspondingly larger. When one considers that the stresses in the 1 mm crystal were sufficient to change the energy dependence of the reflectivity from E^{-1}, as it is in an unstressed crystal, to about E^{-2}, it seems reasonable to assume that the larger stresses in the 2 mm crystal might produce a further change in the energy dependence. A re-evaluation of the reflectivity will require a number of different sources, and cannot be completed for some time.

Intensities of lines measured in the gamma spectrometer were tabulated. However, because of the uncertainty in one of the main corrections, as noted above, these were given no weight* in the final compilation of relative intensities in this decay. Since these measure-

---

* The intensities reported in section IV were determined observations of external conversion electrons. See part B, ii.

ments would constitute a check on the reported intensities at some future time when the correction for reflectivity of the quartz crystal is better known, they are included in an appendix.

iv. Source preparation, gamma

Ir^{192} is produced by thermal neutron capture from the stable isotope Ir^{191}, which comprises 38.5% of naturally occurring Ir. It decays with a half-life of 74.5 days. (1). For the source to be used in the gamma spectrometer, a small rectangular piece was cut from pure Ir metal foil. The dimensions of the piece were 0.463 x 0.044 x 0.005 cm, its total mass was 2.1 mg. The Ir metal was placed in a capillary tube made of fused quartz. The tube was heated and pressed flat, sealing the metal completely. The quartz was then ground to rectangular shape and polished, so that the metal could be clearly seen, and correct alignment in the source holder made. The completed source is diagrammed below.

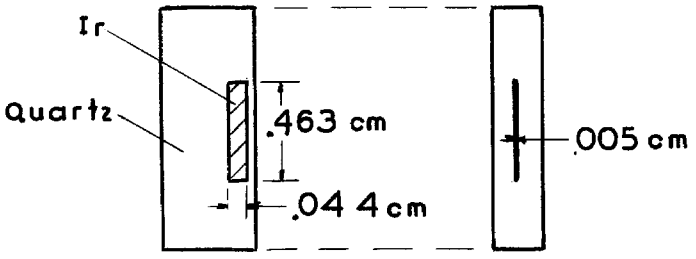

The source was irradiated for 13.7 days in a pile, with a neutron flux of 4.8×10^{13} neutrons/cm^2/sec. This produced an initial activity of ~700 mC.

In addition to Ir^{192}, Ir^{194} is also produced by neutron capture in Ir^{193} (61.5% of natural Ir). However, this activity has a half-life

of only 19 hours, and had decayed below the threshold of observation by the time the source was received in this laboratory. The most likely impurities in Ir metal would be Os and Pt. Activities produced in these elements which should have been observable, had they been present, at the time of the experiments (that is, those which have a half-life longer than one day), include Os^{185} (97 d), Os^{187m} (35 hr.), Os^{191} (16 d), Os^{193} (30 hr.), Pt^{191} (3 d), Pt^{193m} (4.6 d), Pt^{195m} (4 d). None of these was observed.

B. Beta Spectrometer

i. General description

The design of the beta spectrometer follows closely the principles outlined by DuMond for achieving maximum luminosity together with high resolution. (15)(16) It employs a homogeneous magnetic field, produced by field coils wound on the surface of an ellipsoid of revolution, with a constant number of turns per unit length along the major axis. The field is both measured and stabilized by a proton resonance system. A small disc source is placed on the axis of the ellipsoid. Electrons emitted into a small range of angles around 45^{o} with the axis are focussed in a ring, where the resolving slit is placed. They are detected by a thin-window Geiger counter.

The momentum resolution of the spectrometer depends on the size of the electron source, the opening of the resolving slit, and the angle of acceptance. For optimum performance, the contribution to the line width due to each of these causes is matched. (16) The resolution obtained in the investigation reported herein was 0.25 and 0.35% for internal conversion lines, and 0.65% for external conversion lines.

The larger figure with the external conversion lines was due to the size and thickness of the converter (see part iii, Source preparation, beta.)

The resolution of the beta spectrometer, expressed on an energy scale for comparison, gets better at higher energies. It is easily shown that the resolution varies as

$$\frac{dE}{E} = \frac{dp}{p} \quad \frac{(E + 2mc^2)}{(E + mc^2)} = (\text{const.}) \frac{(E + 2mc^2)}{(E + mc^2)}$$

where E is the kinetic energy of the electrons. With a momentum resolution of 0.25%, the resolution, on the energy scale, of the beta and gamma spectrometers is the same at about 250 kev.

ii. Intensity measurements

The only correction applied to intensities of internal conversion lines was that for the sensitivity of the detector. The Geiger counter used had a mica window, 0.7 mg/cm^2 thick. The sensitivity of this counter was determined by measurements on the known beta spectrum of Cs^{137}. (17) It has a cut-off at about 25 kev.

The external conversion line intensities were corrected for:

1. gamma absorption in the source and container,
2. energy dependence of the photoelectric cross section of the converter,
3. anisotropy of photoelectric ejection,
4. efficiency of the detector.

The first two of these are easily calculated if the source geometry is known (see part iii, Source preparation, beta). The third correction requires the tedious calculation of the distribution of photoelectrons

as a function of angle and energy, averaged over the angle of incidence of the gamma rays. This calculation has been carried out by Murray (17), and his results were used.

iii. Source preparation, beta

For internal conversion sources, iridium metal was evaporated in vacuum onto a thin sheet of mica. Small discs, 1 and 1.5 mm in diameter, were punched from this sheet, and attached to the end of an aluminum rod. A thin layer of aluminum was then evaporated over the source to prevent the accumulation of charge on the mica. These sources were thin enough that the lines showed no broadening even at the lowest energies measured.

The assembly of the external conversion source is shown in fig. 4. The source was a very small piece of iridium metal ($\sim$ 0.05 mm, roughly cubic). The converter was uranium, 1.2 mg/cm^2 thick, evaporated on aluminum foil. A 3 mm disc was punched from the foil and cemented on an aluminum cap. The source to converter distance was 0.65 mm.

As a check for impurities, or for unexpected activities produced in the source, a chemical separation of some of the source material was made, by a method due to Meinke. (18) * The end product of this separation was a precipitate, in which the iridium is present as a chloride complex, $IrCl_6^{=}$. A source was prepared by transferring some of this precipitate to a 3 mm mica disc, and evaporating to dryness. No evidence was found for any extraneous activities.

---

* We are indebted to Mr. Floyd Humphrey for performing this separation. A description of the separation is included in Appendix II.

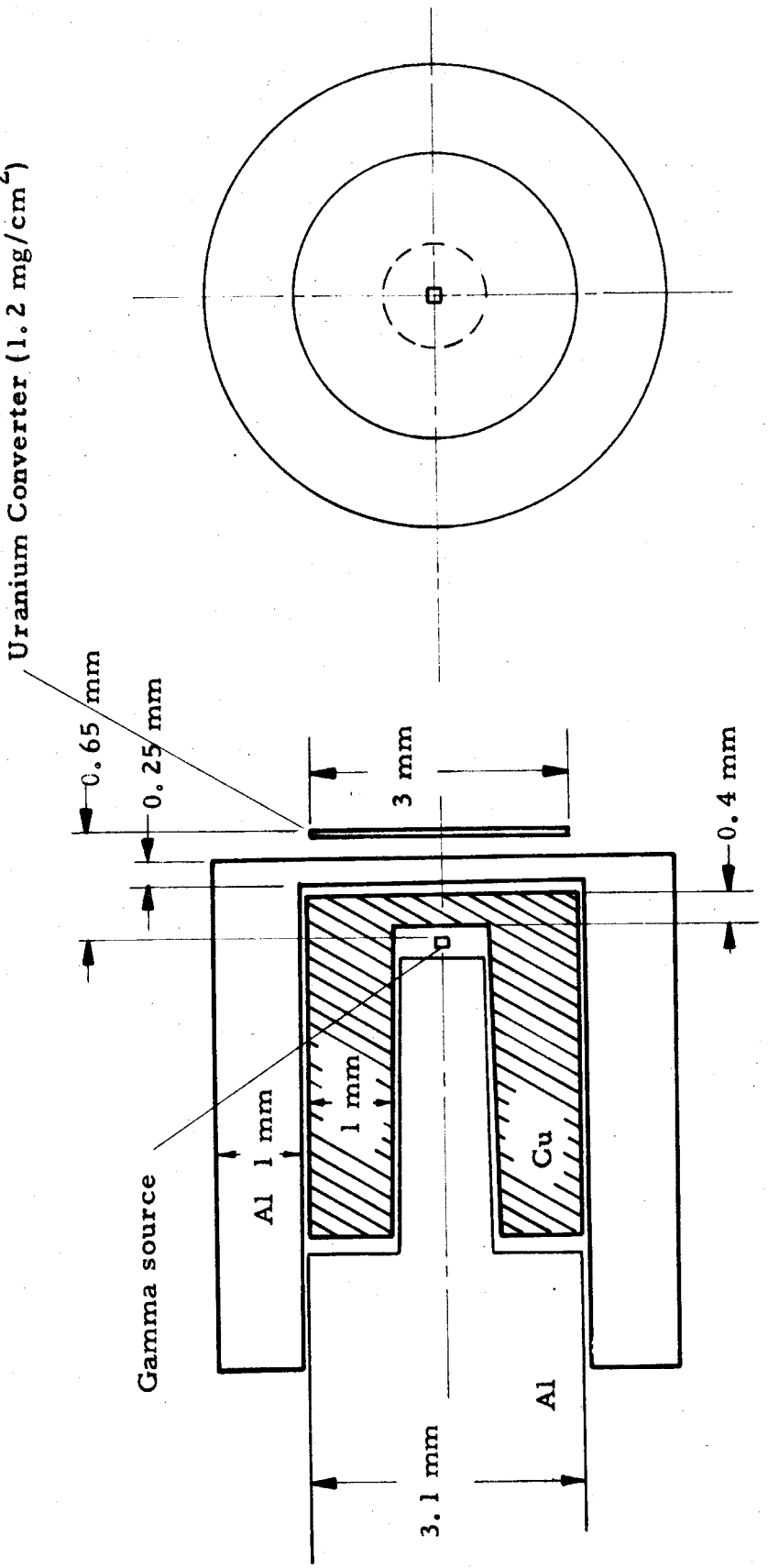

Fig. 4. Assembly of the external conversion source.

C. Scintillation Counters

i. General

Fig. 5 shows a block diagram of the detecting system. The scintillators were two cylindrical crystals of NaI(Tl), 1" diam. x 1/2" thick. They were mounted on the face of DuMont photomultiplier tubes. The pulses from the multipliers were shaped by shorted delay lines to be relatively flat-topped, and 1 μs wide. The amplifiers used two three-tube loop feedback amplifier circuits, with a total gain of 4000. The two single channel differential pulse height discriminators had Schmidt trigger circuits as the discriminating elements. (19) The linearity of the amplifiers and discriminators was carefully checked, and was good up to pulse amplitudes of 80 volts. The coincidence circuit, used in gamma-gamma coincidence and angular experiments, had a resolving time of 0.5 μs. A 2 μs delay could be inserted in one channel for determining the accidental coincidence counting rate.

ii. Intensity measurements

The relative intensities of gamma lines were computed by comparing their photopeaks. The correction for the photopeak efficiency was established in the following manner:

A complete pulse height spectrum of a monoenergetic gamma ray is plotted (fig. 6). The photopeak is separated from the Compton continuum by extrapolating the low energy side of the photopeak so as to make it symmetric with the high energy side. The low energy part of the Compton continuum is extrapolated beneath the backscatter peak* and the X-ray peak as shown (dotted lines).

---

* The backscatter peak comes primarily from radiation scattered into the NaI crystal from the face of the photomultiplier tube behind it. The backscattered radiation from gamma rays of 200 to 1000 kev is concentrated in the relatively narrow region from 110 to 200 kev.

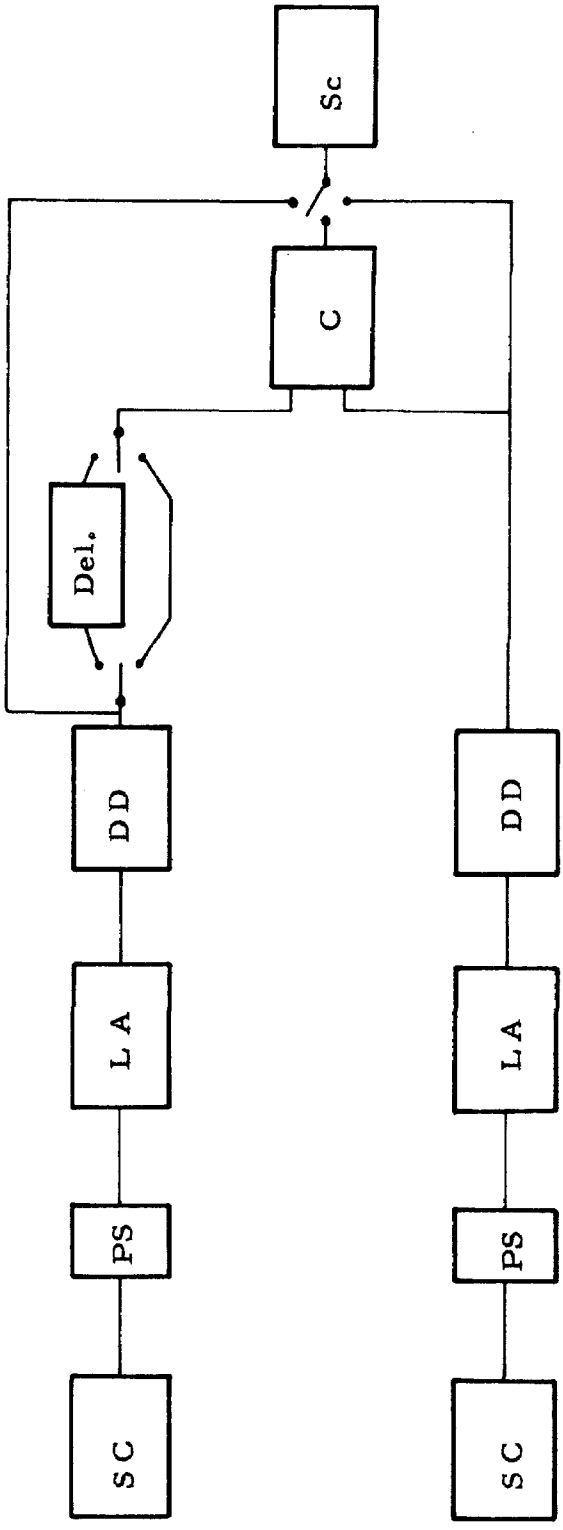

LEGEND

S C : Scintillation Counter

P S : Pulse Shaper

L A : Linear Amplifier

D D : Differential Pulse Height Discriminator

Del : 2 μs Delay

C : Coincidence Circuit

Sc : Scaler

Fig. 5. Block Diagram of Circuitry used for Gamma-Gamma Coincidence and Angular Correlation Measurements.

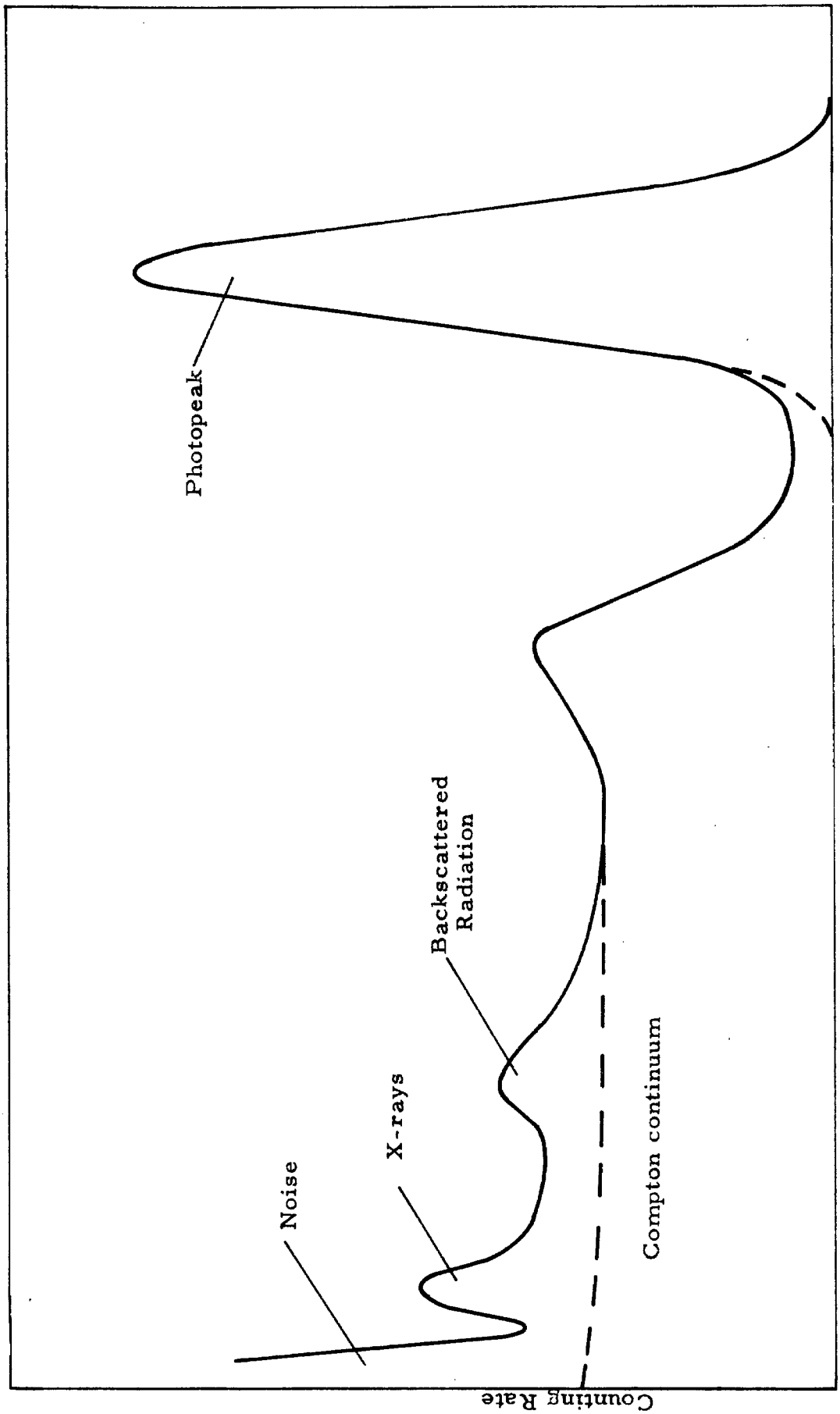

Fig. 6. Typical pulse height spectrum of monoenergetic gamma rays detected by a NaI scintillation counter. The gamma ray energy is 661 kev (Cs^{137})

The numbers of counts in the photopeak, n_P, and in the Compton continuum, n_C, are found.

The total number of counts in such a spectrum is given by the number of incident gamma rays multiplied by the probability of having a primary interaction (photoejection or Compton scattering, below 1 Mev) in the detecting crystal - that is, $n_P + n_C = n_o(1 - e^{-\mu t})$, where n_o is the number of incident quanta, t is the thickness of the crystal, and μ is the linear absorption coefficient. The height of the pulses, however, will depend not only on the primary interactions, but also on secondary and higher order interactions (such as an incident quantum being Compton scattered one or more times, and then ejecting a photoelectron). The photopeak efficiency is given by the ratio of the photopeak counts to the total number of counts, times the probability of a primary interaction, or $(1 - e^{-\mu t})\, n_P/(n_P + n_C)$.

This procedure was carried out for the gamma rays of Hg^{203}, Cs^{137}, Na^{22}, and Co^{60}, covering the energy range from 279 kev to 1.33 Mev. The results, for a crystal 1" in diameter and 1/2" long, are shown in fig. 7.

Maeder, Müller and Wintersteiger (20) have made estimates of the higher order interactions, and their effect on the shape of the spectrum, as a function of energy, of crystal size, and of degree of collimation. The photopeak efficiency, calculated by their method, is also shown in fig. 7. For energies above 200 kev, the calculated efficiency diverges from the measured efficiency. The slopes of the two curves are nearly equal, but the calculated efficiency is always the larger by a factor of ~ 1.7. The origin of the difference is not clear. However, the correction for relative intensities depends only

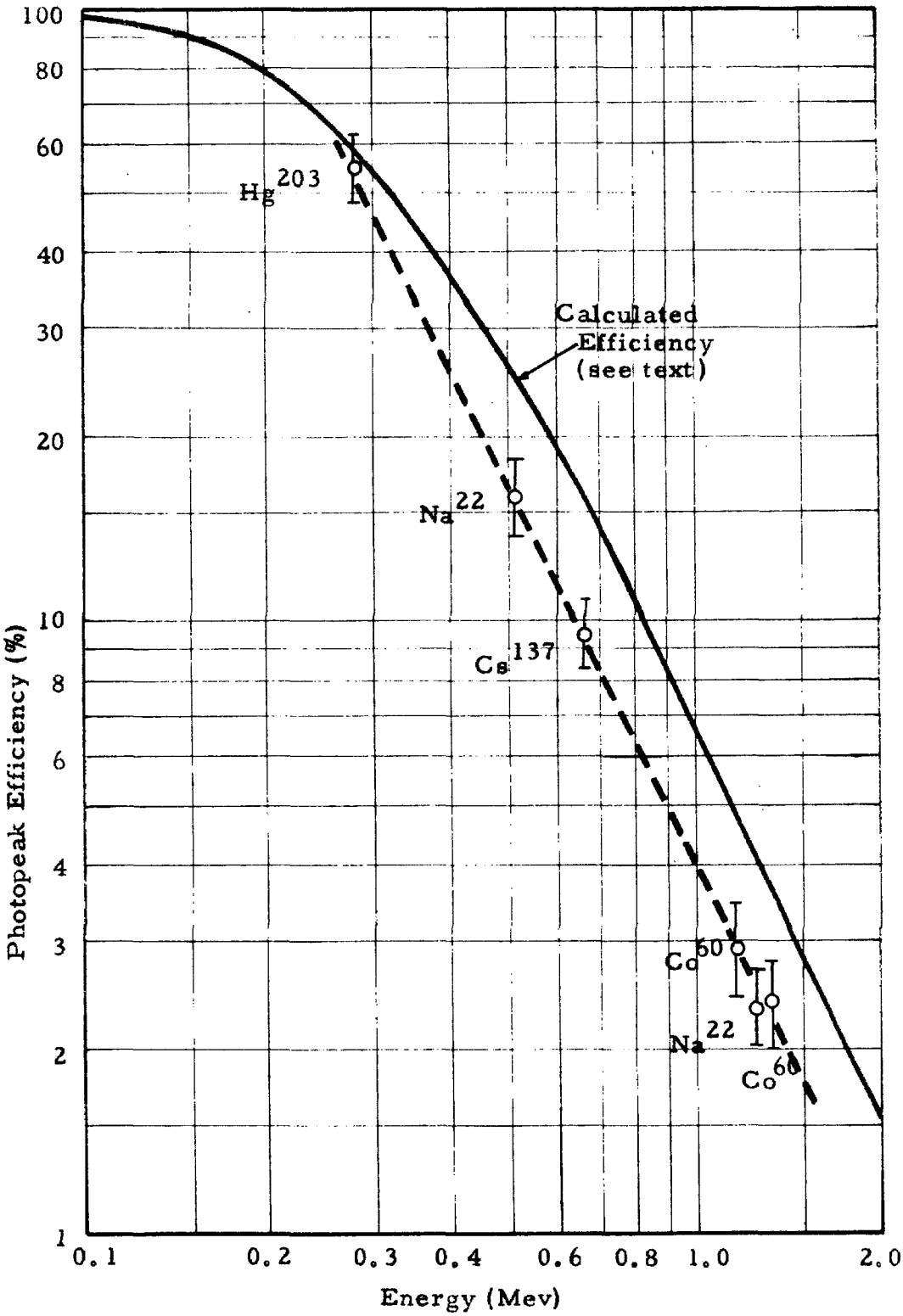

Fig. 7. Photopeak efficiency of a NaI crystal, 1" diameter x 1/2" thick, as a function of energy.

on the slope of the efficiency curve, and not on its magnitude, so this difference will have little effect on the results quoted here.

D. Angular Correlation

Consider a nucleus which emits two successive gamma rays, CB and BA (diagram a). It is well known that if the lifetime of the

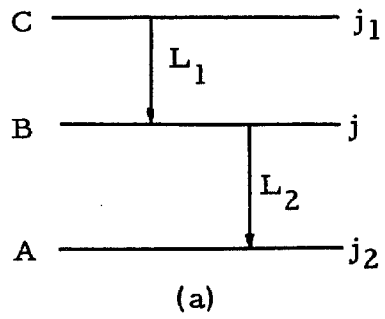

(a)

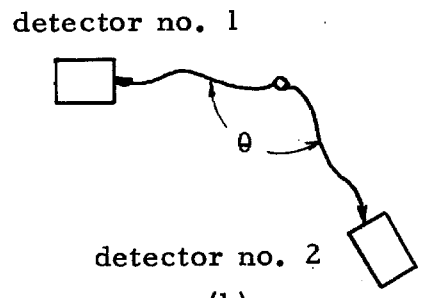

(b)

intermediate state, B, is short compared with the time required for the nucleus to change its orientation in space under the influence of external fields, then the directions of the two gamma rays will not, in general, be independent. (21)(22)(23) If one measures coincidences between the two gamma rays as a function of the angle θ between the two detectors (diagram b), then the coincidence counting rate, C, can be written as a constant times a correlation function, $C = k\, W(\theta)$. $W(\theta)$ will depend on the multipolarities, L_1 and L_2, of the gamma rays, and on the spins of the states involved.

The correlation function can be expressed as a series of Legendre polynomials of even order,

$$W(\theta) = \sum_{k=0}^{n} a_{2k} P_{2k}(\cos\theta) \quad ; \quad a_o = 1$$

It can be shown that n, half the highest order included, must be less than or equal to the smallest of the two multipolarities and the spin

of the intermediate state - that is, $n \leq L_1, L_2, j$. The expansion coefficients, a_{2k}, have been tabulated by Biedenharn and Rose, among others, for most values of L_1, L_2, j, j_1, and j_2 of physical interest. (23)

The theoretical correlation function is derived with the assumption of point source, point detectors, and undisturbed intermediate states. The first condition was fairly well fulfilled, the linear extension of the source being less than 3 mm in all cases. The correction for the finite size of the detectors, following the method of Rose (24), was applied to the theoretical correlation function before comparison with the experimental data. Rose shows that, for a correlation function expanded in Legendre polynomials, the correction for detector size can be expressed as additional coefficients, C_{2k}, which depend only on the source-detector geometry. The observed correlation should then be given by

$$W'(\theta) = \sum_{k=0}^{n} C_{2k}\, a_{2k}\, P_{2k}(\cos\theta).$$

Observations were made with source-to-detector distances of 3 cm and 5 cm. The correction coefficients for these two cases were:

	d = 3 cm	d = 5 cm
C_2/C_o	0.836	0.928
C_4/C_o	0.494	0.799

If the lifetime of the intermediate state is sufficiently long ($\sim 10^{-11}$ sec.), external fields will tend to disturb the angular correlation between the two gamma rays. (25) The fields at the nucleus are strongly affected by the physical and chemical form of the source material. In order not to be misled by such effects, three sources

were used, having quite different forms: Ir metal, evaporated on mica (see II.B., part iii, Source preparation, beta); a precipitate in which the Ir is in a chloride complex, $IrCl_6^{=}$; a solution in concentrated HCl. The results from all three sources were consistent to within the accuracy of the experiment.

The arrangement of the apparatus used for the angular correlation measurements is shown in fig. 8. Two scintillation counters were used, one fixed in position, the other mounted on a movable arm which could be pivoted about a central post. The angle between the two arms was varied in steps of 30^{o} or 45^{o} between 90^{o} and 270^{o}. The source was mounted on the central post, in an aluminum container. Centering of the source was checked by measuring the counting rate, of the movable detector alone, as a function of angle. This counting rate was constant to within 1%.

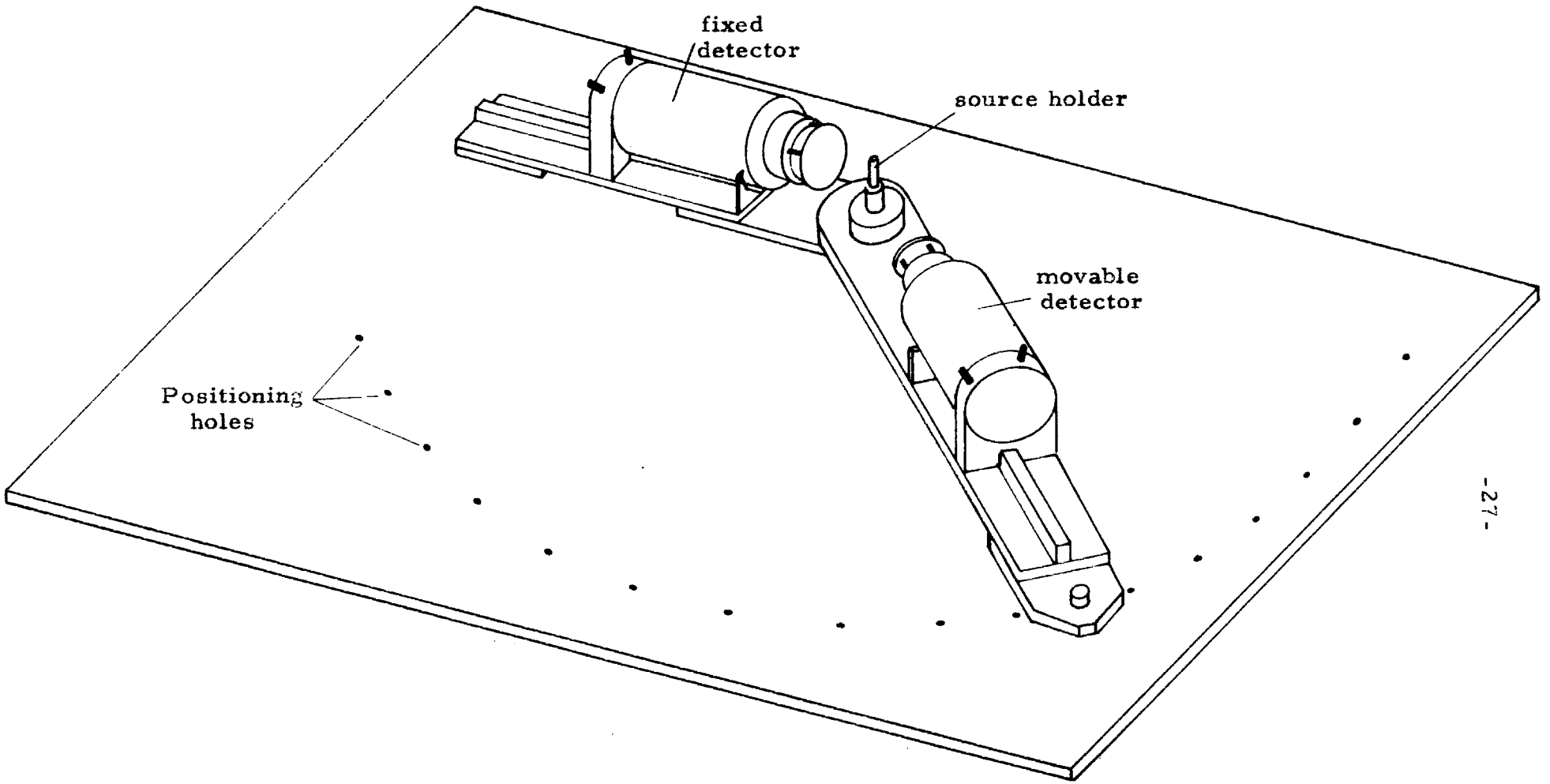

Fig. 8. Physical arrangement of scintillation counters for gamma-gamma angular correlation.

IV. Experimental results

It has long been known that neutron bombardment of natural iridium produces two activities, (26)(27)(1) with half-lives of 19.0 ± 0.2 hours (28) and 74.37 ± 0.07 days (29). These two activities have been identified as Ir^{194} and Ir^{192}, respectively (30). Ir^{192} decays by beta emission to Pt^{192}, and by electron capture to Os^{192} (31).

The major results of this investigation of the decay of Ir^{192} have been collected in Table I and figures 9 and 10. Tabulated in Table I are the measured energies of gamma rays, their isotope assignments, their relative intensities, the relative intensities of their internal conversion lines, their experimental and theoretical internal conversion coefficients, their multipolarity assignments and their decay fractions. Figure 9 presents the proposed energy level scheme of Pt^{192}. Fig. 10 includes three alternative energy level schemes, each of which is consistent with the experimental data.

The balance of this section will be devoted to an exposition of the experimental evidence for these results.

A. Energy measurements

The energies given in Table I, except for the three lines at 785, 885, and 1060 kev, were measured with the gamma spectrometer. The K-conversion line of the 885 kev gamma ray was observed with the beta spectrometer. The 785 and 1060 kev lines were observed only by scintillation counter.

The errors in the energies which are shown in Table I correspond to 1/20 of the line width at half-maximum for strong lines measured with the gamma spectrometer. The error assigned to the weak 283.35,

TABLE I

Gamma Rays of Ir^{192}

Element	Gamma energy E	Gamma intensity I (5)	Conversion intensities I_β (5) K	L_I+L_{II}	L_{III}	Conversion Coefficients a_K(7) exp.	the. E2	the. M1	$a_{L_I+L_{II}}$ exp.	the. E2	the. M1	$a_{L_{III}}$ exp.	the. E2	the. M1	$a_{tot.}$	Decay Frac.	Multi-pol.
Pt	136.33±0.02	0.19	0.19	0.12	0.083	1.0	0.43	2.8	0.63	0.54	0.43	0.44	0.32	0.001	2.07	0.5	E2
Os	201.31±0.04	0.46	0.14	0.05^5	0.033	0.30	0.165	0.98	0.12	0.090	0.12	0.07	0.04	0.0005	0.49	0.5	E2(+M1)
Os	205.75±0.04	3.9	0.64	0.030	0.15	0.16	0.158	0.94	0.077	0.085	0.11	0.04	0.034	0.0005	0.28	4.1	E2
Os	283.35±0.20	0.6	0.02	-	-	0.04	0.070	0.39	-			-			0.04	0.5	(E2)
Pt	295.94±0.09	36	2.35	0.89	0.22	0.065	0.063	0.35	0.025	0.024	0.052	0.006	0.007	2	0.096	32	E2
Pt	308.45±0.09	35	2.42	0.99	0.29	0.069	0.057	0.31	0.028	0.021	0.048	0.008	0.006	0.0002	0.105	32	E2
Pt	316.46±0.09	100	5.40	1.76	0.62 (6)	0.054	0.054	0.29	0.018	0.019	0.045	0.006	0.005	0.0002	0.078	89	E2
(Os)(1)	374.7 ±0.5	1.9	-	-	-	-			-			-				1.6	-
Pt	416.6 ±0.7	1.6	0.031	-	-	0.019	0.028		-			-			0.019	1.3	(E2)
Pt	467.98±0.22	64	1.39	0.33	0.08	0.022	0.022		0.0052	0.0056	0.020	0.001	0.0009		0.028	54	E2
Os	484.75±0.23	3.9	0.087	-	-	0.022	0.019		-			-			0.022	3.3	E2
Pt	588.4 ±0.6	7.1	0.077	0.022	-	0.011	0.0136		0.0031	0.0032	0.012	-			0.014	5.9	E2
Pt	604.5 ±0.9	14	0.224	0.044	-	0.016	0.0123	0.052	0.0031	0.0029		-			0.019	12	E2(+M1)
Pt	612.9 ±0.9	8.4	0.094	0.019	-	0.011	0.0124		0.0023	0.0028		-			0.013	7	E2
(Pt)(2)	785 ±20	<0.1	-	-	-	-			-			-			-	-	-
Pt(3)	885 ±2	0.5	0.0034	-	-	0.007	0.006	0.015	-			-			0.007	0.4	(E2)
(Os)(4)	1060 ±30	0.05	-	-	-	-			-			-			-	0.04	-

(1) 374.7 kev line observed only with the gamma spectrometer. Its K-conversion line falls on the 308.45 and 316.46 kev L lines.
(2) Observed only by scintillation counter.
(3) Observed in beta spectrometer and scintillation counters.
(4) Observed only by scintillation counter.
(5) All intensities are relative intensities.
(6) a_K of the 316.46 kev line was assumed to have the theoretical value for an E2 transition. See part IV, D, Normalization of conversion coefficients.
(7) Theoretical conversion coefficients taken from references (44) and (45).

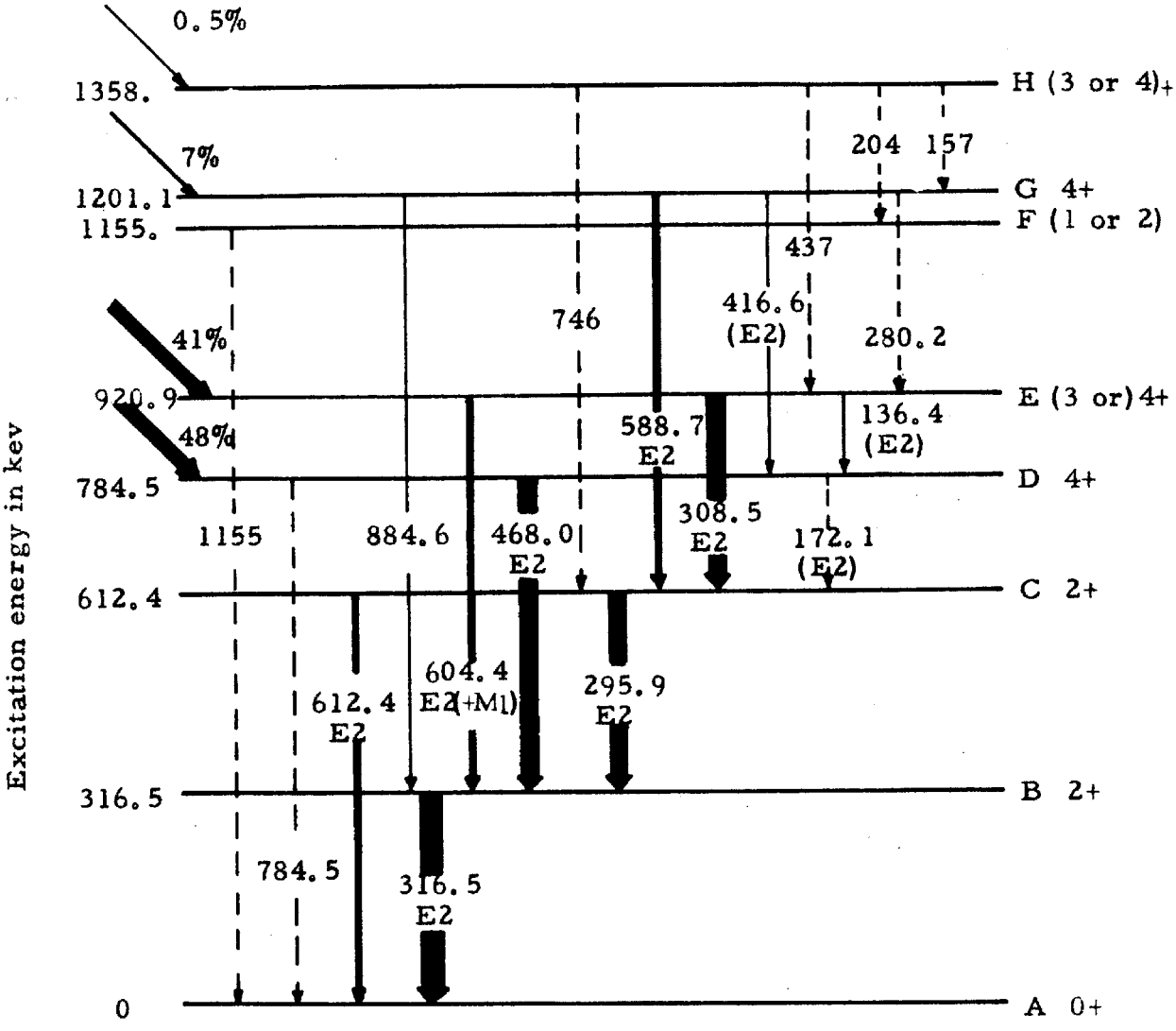

Fig. 9. Proposed energy level scheme for Pt^{192}. The dotted lines indicate gamma ray reported by other investigators, but not found in this laboratory.

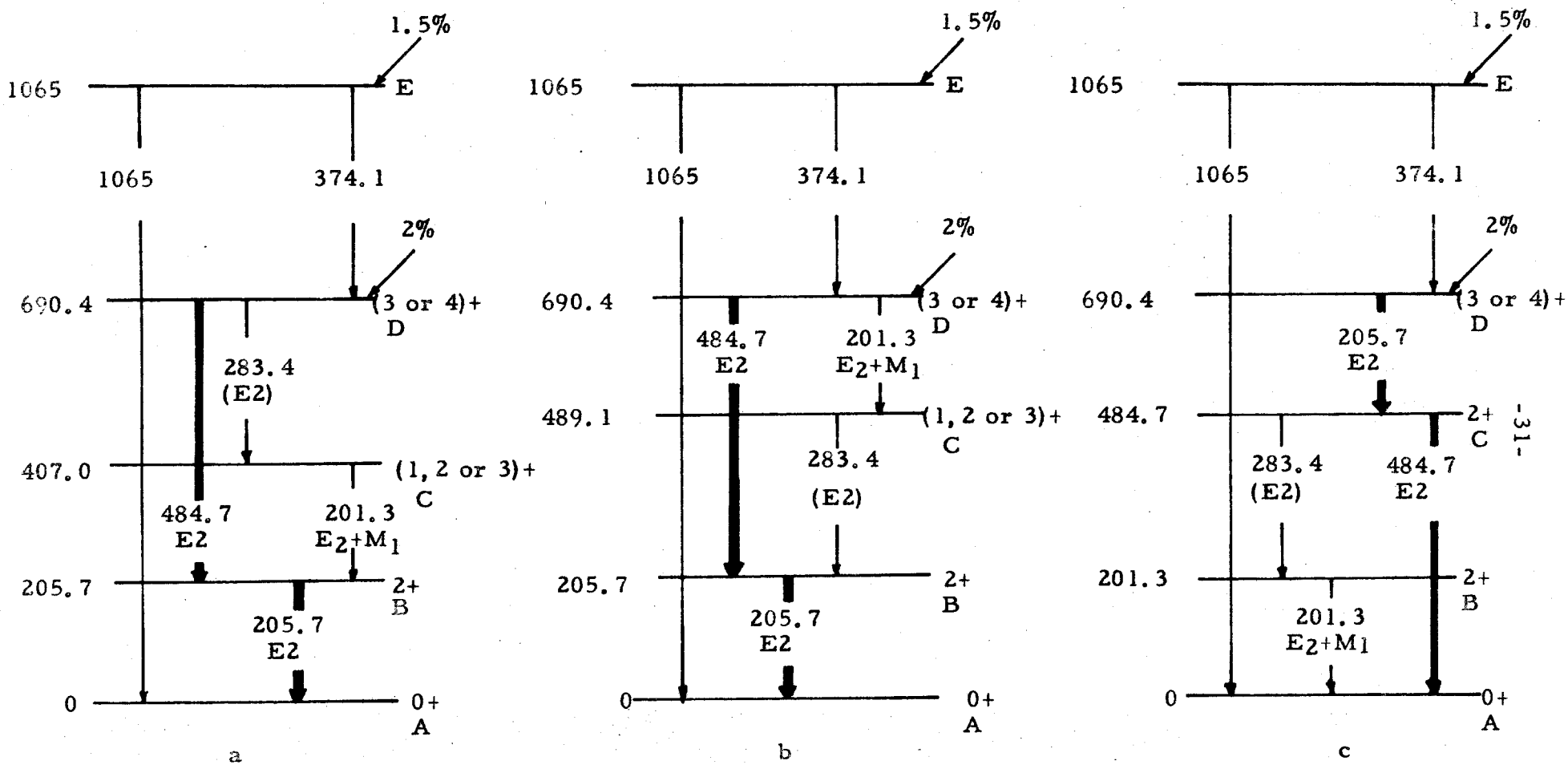

Fig. 10 Proposed energy level schemes for Os^{192}. (See Section IV, part F).

374.7 and 416.6 kev lines corresponds to 1/5 the line width. The error given to the two lines observed by scintillation counter, the 785 and 1060 kev lines, is $\pm 3\%$. The error assigned to the 885 kev line is 1/2 the line width in the beta spectrometer.

The energy measurements agree well with those of Johns and Nablo (32) and with those of Cork's group (31). Their values have been tabulated in Table II to allow easy comparison. Also included in Table II are the energy measurements of the gamma rays found in the decay of Au^{192}, by Ewan and Thompson (33). Au^{192} decays by electron capture and positron emission to Pt^{192}.

There are eight lines which have been reported by one or more of the three groups cited above, which have not been observed here. Seven of these lines (all except the one at 400 kev) have been incorporated in the decay scheme shown in fig. 9, where they appear as the broken lines.

B. Intensities

The gamma intensities given in Table I are based primarily on measurements of external conversion lines with the beta spectrometer (sect. III.B, part ii). Intensity ratios of lines within closely-spaced groups have been determined or verified by gamma spectrometer measurements (sect. III.A, part iii). These include the ratios of intensities of the following lines: 201 - 205; 296 - 308 - 316; 468 - 484; and 588 - 604 - 613 kev. In the scintillation counters, each of these groups of lines appears as an unresolved peak (fig. 11). The integrated intensities of these unresolved groups of lines were checked by measurements with the scintillation counters. The intensities of the 885 and 1060 kev lines were determined by scintillation counter measurement

TABLE II

Gamma Ray Energies

Element	This investigation	Johns, Nablo	Cork	Ewan, Thompson (Au^{192})
Pt	136.33 ± 0.01	136.2 ± 0.3		
Pt			156	157.7
Pt		174.0 ± 0.4	173	173.4
Os	201.31 ± 0.04	201.2 ± 0.3	201.1	
Os	205.75 ± 0.04	205.4 ± 0.2	205.74	
Pt				205.4
Pt		281.5 ± 0.5		281.8
Os	283.35 ± 0.20		283	
Pt	295.94 ± 0.09	295.8 ± 0.1	294.9	295.7
Pt	308.45 ± 0.09	308.4 ± 0.1	307.7	308.1
Pt	316.46 ± 0.09	316.5 ± 0.1	316.1	316.0
(Os)	374.7 ± 0.5	374 ± 2		
-			400	
Pt	416.6 ± 0.7		415.1	415.5
Pt		440 ± 2	438	
Pt	467.98 ± 0.22	467.8 ± 0.1	467.4	467
Os	484.75 ± 0.23	484.4 ± 0.2	484	
Pt	588.4 ± 0.6	588.7 ± 0.3	588.6	588
Pt	604.5 ± 0.9	604.5 ± 0.3	603.7	
Pt	612.9 ± 0.9	612.7 ± 0.2	611.2	612
(Pt)		745 ± 3		
Pt	785 ± 15	783 ± 2		783
Pt	885 ± 2	885.4 ± 1.0		
(Os)	1060 ± 20	1065 ± 2		
Pt		1157 ± 2		1158

alone.

The error in the gamma intensities is estimated to be ± 20% for lines with an intensity greater than 2.0, and 30 to 50% for the weaker lines.

C. Isotope assignment

Several different means were employed to assign the gamma rays either to the Pt branch or to the Os branch of the decay. Wherever possible, the assignment was made by comparing the energies of the gamma rays, as determined by gamma spectrometer measurements, with the energies of the K-conversion lines, as measured with the beta spectrometer. Since the difference in binding energy of the K electrons in these two elements, 4.5 kev, lies well outside the range of error of energy measurement, this method is very reliable. Isotope assignments for thirteen of the seventeen gamma rays listed in Table I were made in this manner.

The 885 kev line was assigned to Pt on the basis of observed coincidences between it and the 316 kev line of Pt (see part E).

If a line is observed in the decay of Au^{192}, it must belong to the Pt branch. On this basis, the 157, 281.8, 783 and 1155 kev lines have been assigned to Pt. A line at 205.4 kev has been reported in the Au^{192} decay, which would indicate that a line of this energy is found in the Pt branch. However, the line observed at 205.75 kev in this laboratory can be definitely assigned to the Os branch by the energy of its K-conversion line. Therefore, a line of this energy must be found in both branches. Ordinarily, this would be easy to check, by looking for two K-conversion lines separated by 4.5 kev. However, there is another

Os line just 4.45 kev lower in energy, at 201.30 kev, whose K-conversion line coincides with the expected conversion line of the Pt 205.7 kev gamma ray. For this reason, it was impossible to verify the presence of a 205 kev gamma ray in Pt.

Finally, when all the assigned gamma rays have been combined into a tentative decay scheme, one can try to fit the remaining lines into one or the other branch of the decay. It is easy to see that this is less reliable than any of the other methods, and assignments made on this basis have been enclosed in parentheses, to indicate their tentative status. The lines so assigned include those at 374.7, 745 and 1060 kev. (The 374.7 kev line was observed only with the gamma spectrometer. Its K-conversion line falls among the L-conversion lines of the intense 296 - 308 - 316 kev group.)

The 400 kev line could not be assigned.

D. Normalization of internal conversion coefficients

The classification of gamma rays according to multipolarity is most frequently made by measuring the internal conversion coefficients of the transitions, or the ratios of conversion coefficients - such as the K/L ratio, the $(L_I+L_{II})/L_{III}$ ratio, etc. (34). If, for a group of gamma rays (labelled by the subscript n), one experimental method yields the relative gamma intensities, $I_{\gamma n}$, and by another experimental method the relative internal conversion intensities, $I_{\beta n}$, are known, then the internal conversion coefficients are given by

$$\alpha_n = k \frac{I_{\beta n}}{I_{\gamma n}}$$

in which k is a constant for all the transitions. The ratios of the conversion coefficients are, of course, independent of the normalizing

constant. If it can be determined that one of the gamma rays is an unmixed multipole transition, and its multipolarity can be established (by the K/L or $(L_I+L_{II})/L_{III}$ conversion ratios, for instance) then the conversion coefficients for that transition can be set equal to their theoretical values, thus fixing the value of k.

The conversion coefficients given in Table I have been determined by such a procedure. The 316 kev line is the most intense line in the decay. Its K, L and M conversion peaks are all clearly observable. The experimental K/L conversion ratio for this line is 2.3, and its $(L_I+L_{II})/L_{III}$ conversion ratio is 3.0. The theoretical conversion ratios for E1, E2, M1 and M2 transitions are:

	K/L	$(L_I+L_{II})/L_{III}$
E1	5.0	8.1
E2	2.3	3.8
M1	6.5	220
M2	4.6	17

The experimental ratios fit best with the theoretical ratios for an E2 transition. Furthermore, the 316 kev line is almost certainly a transition to the ground state of Pt (see part F). Pt^{192} is an even-even nucleus, whose ground state spin is assumed to be 0. Therefore, a transition to this state must be a pure multipole transition.

On the basis of the above arguments, the K conversion coefficient of the 316 kev line was given its theoretical value of 0.054 (34). The relative internal conversion intensities were so normalized that the constant k had the value 1.

All the multipolarity assignments were E2 or E2+M1, indicating that there is no parity change throughout the energy level scheme.

E. Coincidence measurements

The Ir^{192} gamma ray spectrum, as seen with a scintillation counter, is shown in figs. 11 and 12. The peaks have been labelled the X-ray, "backscatter", "200", "300", "470", "600", "785", "885", and "1060" peaks. The first six of these are known to be complex peaks, each including two or more unresolved lines. The X-ray peak contains the K X-rays of Os, Ir, Pt and Pb (the latter due to fluorescence in the shields which surround the source and detectors). The backscatter peak comes primarily from radiation scattered into the NaI crystal from the face of the photomultiplier tube behind it. The backscattered radiation from lines at 200 to 600 kev is concentrated in the relatively narrow region of 110 to 180 kev. The backscatter peak completely obscures the line at 136 kev. The "200" peak contains the two lines at 201 and 205 kev; the "300" peak includes the three lines at 296, 308 and 316 kev; the "470" peak, those at 467 and 484 kev; the "600" peak, those at 588, 604 and 613 kev. The "785", "885", and "1060" peaks are probably simple.

Because so many of the lines are unresolved, what is actually observed in the coincidence measurements is coincidences - or lack of coincidences - between one or more lines in one group and one or more lines in another group.

The results of the coincidence measurements are tabulated in Table III. The column headings correspond to the peaks in figs. 11 and 12. In all cases, the coincidences observed are consistent with the proposed energy level schemes.

Two cases were particularly interesting in that the coincidence peaks were noticeably shifted from the single counts peaks. With one

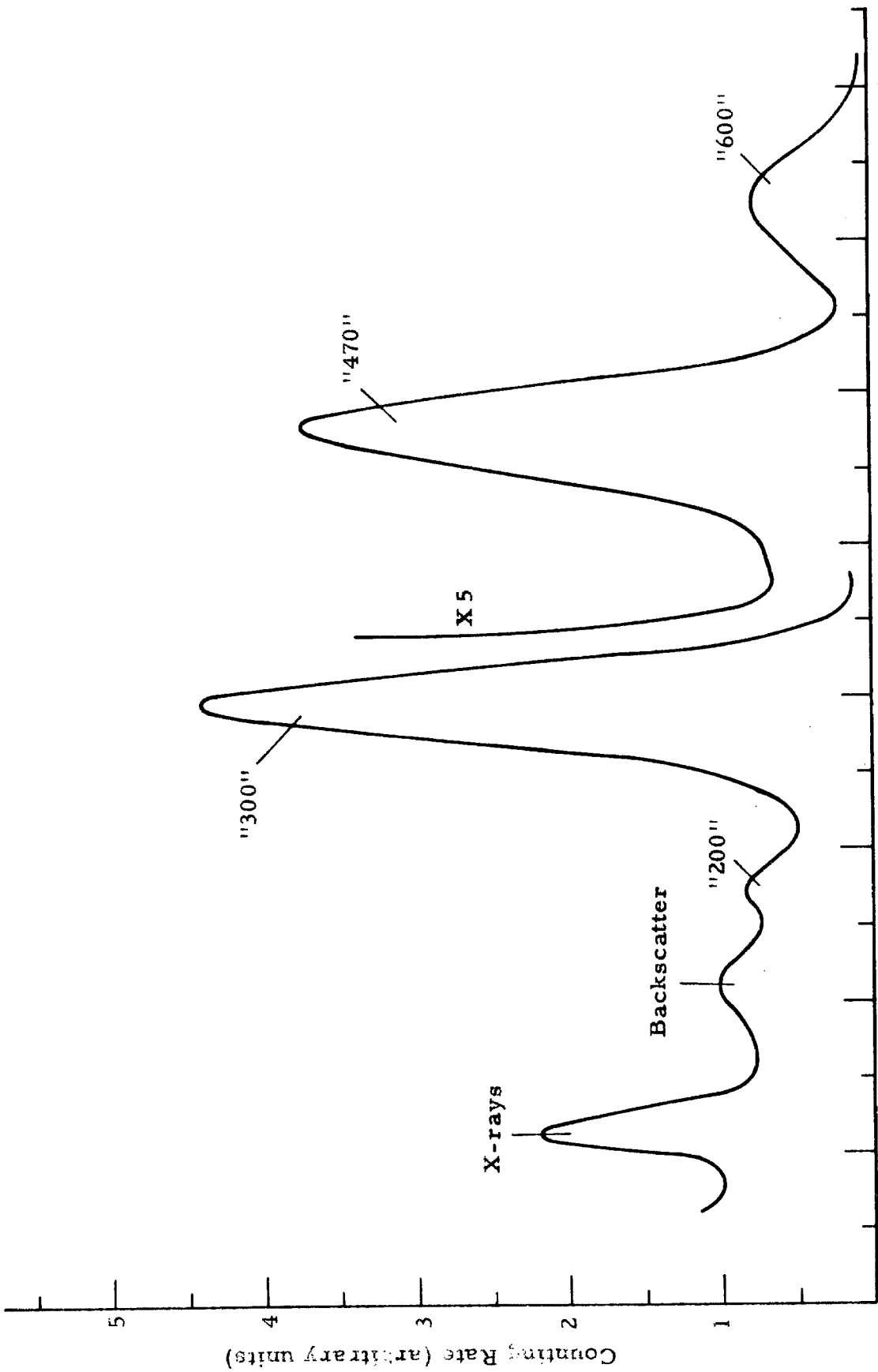

Fig. 11. Part of the gamma-ray spectrum of Ir^{192} as seen with a scintillation counter.

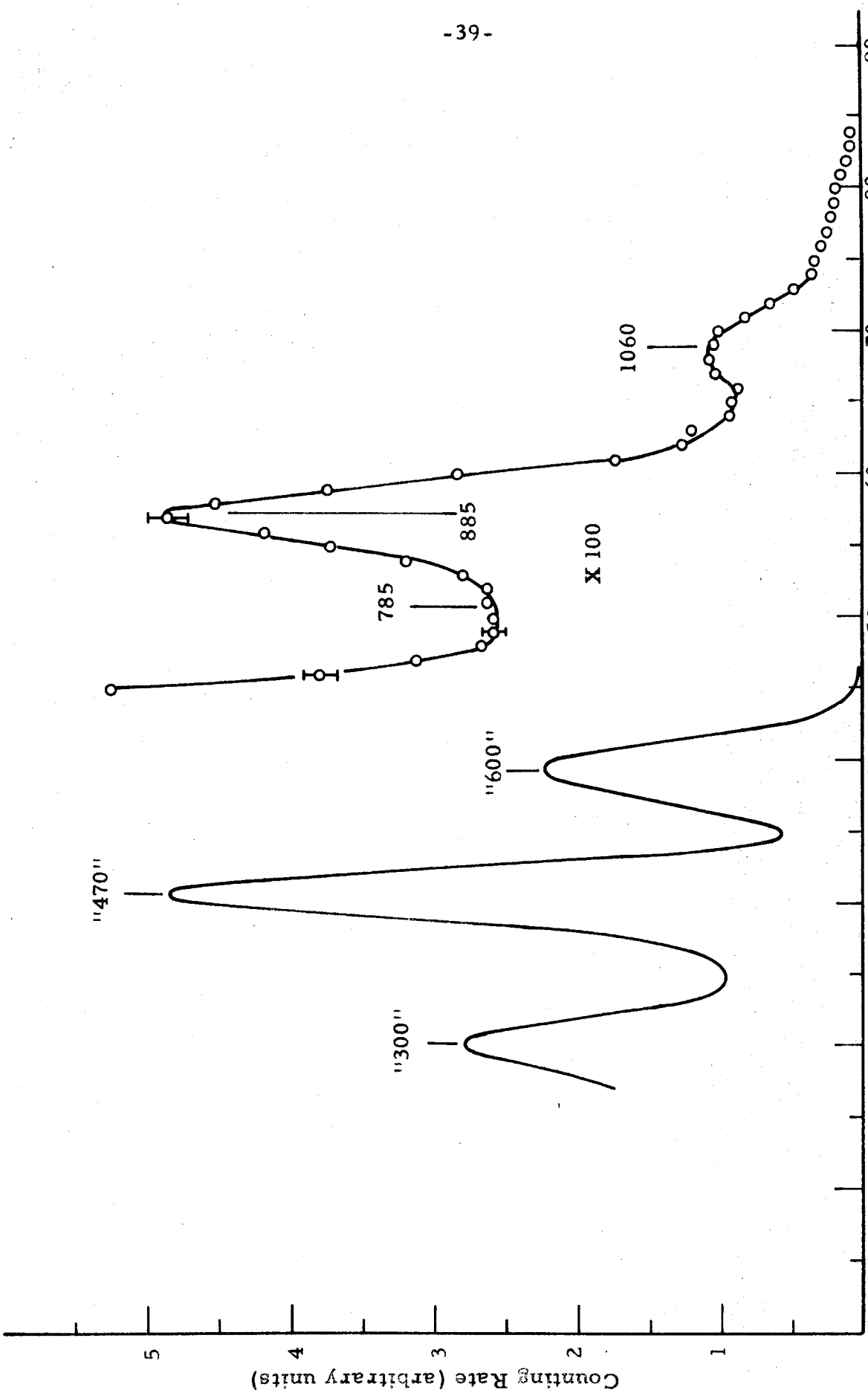

Fig. 12. Gamma-ray spectrum of Ir^{192} after passing through 1.38 cm of Pb, showing the weak, high energy lines.

TABLE III

Coincidences Between Groups of Gamma Lines

(The column headings correspond to the labels found in figures 11 and 12.)

	"200" (1)	"300" (2)	"470" (3)	"600" (4)	"785"	"885"
"200"	yes	no	yes**	no	-	-
"283"*	yes	-	-	-	-	-
"300"	no	yes	yes	yes	no	yes
"470"	yes	yes**	no	no	-	-
"600"	no	yes	no	yes	-	-

(1) Includes 201.3 and 205.7 kev lines

(2) Includes 295.9, 308.4, and 316.5 kev lines

(3) Includes 468.0 and 484.7 kev lines

(4) Includes 588.4, 604.5 and 612.9 kev lines

* Fixed channel set just at the low-energy foot of the "300" peak.

** Peak is shifted toward high energy from single-counts peak (see text).

channel set to accept pulses from the "470" peak, the second channel was moved stepwise over the "300" peak. Both coincidence counts between the two channels and single counts in the second channel were recorded. The results are plotted in fig. 13. The coincidence peak is distinctly shifted toward high energy from the single counts peak. This is consistent with the energy level scheme of fig. 9, according to which the 467 kev line should be in coincidence with the 316 kev line, but not with the 296 or 308 kev lines.

A similar shift toward high energy was noted in the "470" peak observed in coincidence with the "200" peak. This is consistent with the level scheme of fig. 10, which indicates the 205 kev line is in coincidence with the 484 kev line, but not with the 468 kev line of Pt.

F. Energy levels

The proposed arrangement of the energy levels in Pt^{192} is shown in fig. 9. The weak transitions which have not been observed in this laboratory are shown as broken lines. The two levels F and H, at 1155 and 1358 kev, depend entirely on these weak transitions, and therefore their existence is somewhat uncertain. Except for these two levels, no other arrangement has been found which does not introduce serious conflict with coincidence or intensity data.

This arrangement of levels agrees with that proposed by Johns and Nablo, who based their proposal on energy and intensity considerations alone. The arrangement is also consistent with the results of Lu and Wiedenbeck (35), who observed the so-called sum peaks of Ir^{192} with a well-type scintillation counter.*

* A well-type scintillation counter is one in which the detecting crystal has a hole drilled into its center. With a source placed in the "well", there is a high probability that gamma rays emitted in cascade will be captured simultaneously, producing a pulse corresponding to the sum of the energies of the gamma rays. These pulses form the so-called sum peaks.

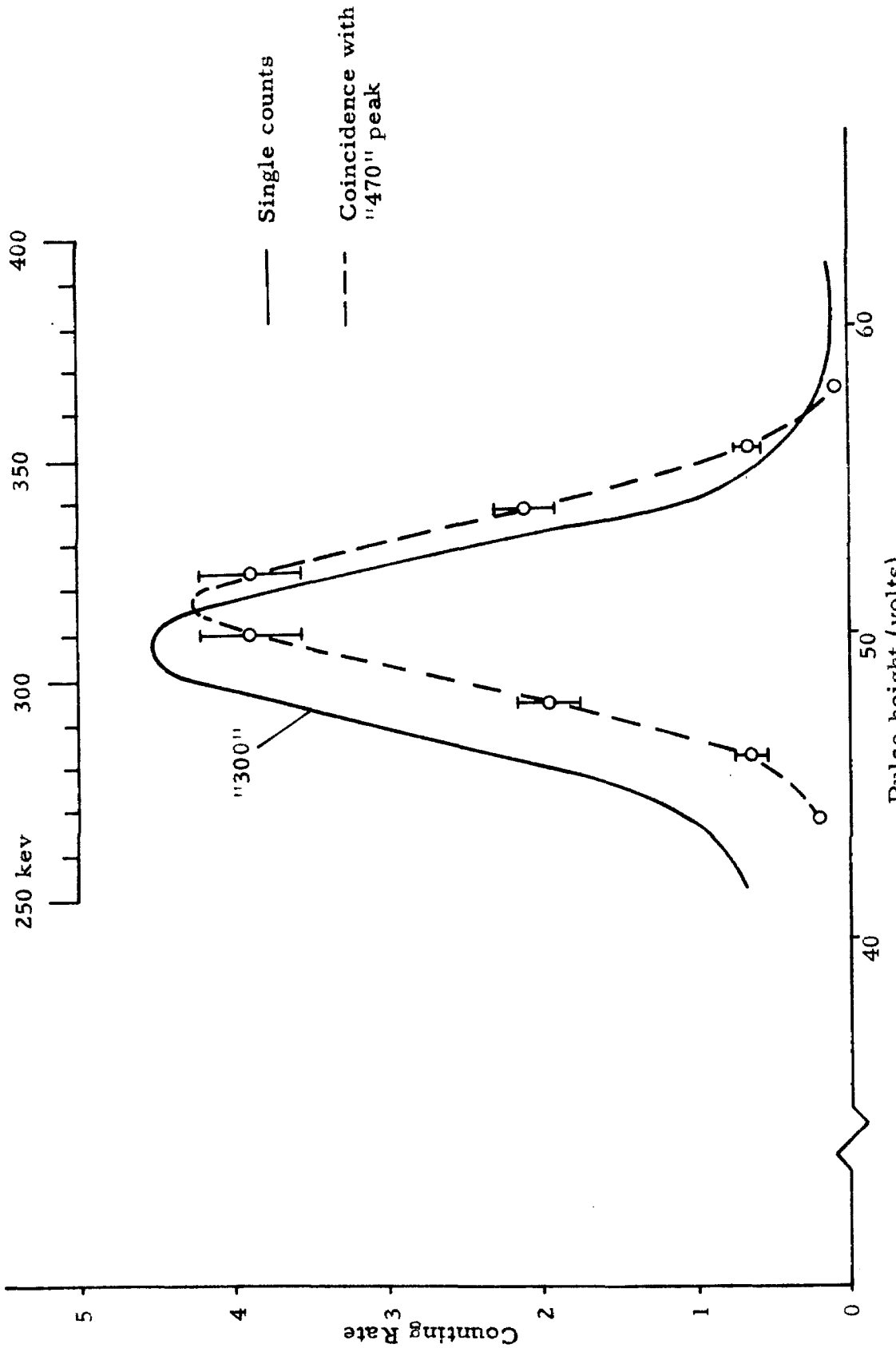

Fig. 13. Showing the "300" kev peak as seen by a single counter, and in coincidence with the "470" kev peak.

The proposed arrangements of energy levels in Os^{192} are shown in fig. 10. There are three alternative arrangements of the first four levels, all of which are consistent with all the coincidence and intensity data. The first excited level in the proposed schemes lies either at 205.7 kev (schemes 10 a and b) or at 201.3 kev (scheme 10 c). They differ in this respect from the schemes which have been reported in the literature (31)(32)(42), all of which have the first excited level at 283 kev.

The evidence about the proper arrangement is found in the Coulomb excitation studies made by Temmer and Heydenburg (36)(37). Exciting natural Os with 6 Mev alpha particles, they observed the subsequent gamma rays with a scintillation counter. They found peaks at 155 and 200 kev. The 200 kev peak is broader than would be expected for a simple line, and probably contains two or more lines. They see no evidence of a peak at 283 kev.

There are seven stable isotopes in natural Os, of which Os^{192} is the most abundant (41.0%). Os^{192} has two gamma rays at 201 and 205 kev. Os^{188} (13.3%) has a known first excited level at 156 kev (38). Nijgh, et al (39), have reported strong conversion lines at 112 and 172 kev in the spectrum of Ir^{190}, which decays by electron capture to Os^{190}. These can be interpreted as the K and L conversion lines of a 186 kev gamma ray in Os^{190}. (Os^{190} makes up 26.4% of natural Os.) No information is available about the energy levels of Os^{189} (16.1%). The other three stable isotopes, Os^{184} (0.018%), Os^{186}(1.59%), and Os^{187} (1.64%) are present only in small quantities. We conclude that the observed gamma rays are due to excitation of the 156 kev level of Os^{188}, a 186 kev level in Os^{190}, and a level at about 200 kev in Os^{192}, and that

other effects are small, or at least not large enough to alter materially the above conclusions. The measurements are not sufficiently precise to distinguish between a level at 201 kev and one at 205 kev. It is clear, however, that the first excited level of Os^{192} cannot be as high as 283 kev.

The 201.3 kev transition seems to be a mixed E2+M1 transition (Table I). The admixture seems to be $\sim$80%E2 and $\sim$20% M1. This fact throws some doubt on the scheme of fig. 10c, since the ground state transition should be unmixed. However, this evidence is not felt to be strong enough, in the absence of other data, to finally reject the scheme of fig. 10 c.

G. Decay fractions and comparative half-lives

The decay fractions into and out of the various levels shown in figs. 9 and 10 are tabulated in Table IV. The relative decay fraction of a transition is given by $I_\gamma(1+\alpha_{Total})$. The decay fractions were normalized so that the sum of the ground state transitions (316, 612, 783 and 1155 kev in Pt, 205 and 1060 in Os) was 100.

i. Pt^{192}

In the Pt branch, the decay fractions indicate the presence of four beta groups, with relative intensities 48: 41: 7: $<$0.5, going to levels D, E, G and H, respectively. The end point of the most energetic group was measured as 673 $\pm$ 10 kev. This agrees well with the previous measurements of Johns and Nablo, 672 kev; of Levy (40), 670 $\pm$ 13 kev; and of Spinel and Forafontov, (41), 660 $\pm$ 10 kev. If this is identified as the energy of the beta transition to level D, the resulting value of the Ir^{192} - Pt^{192} mass difference is 1457 $\pm$ 10 kev. This agrees reasonably

TABLE IV

Decay Fraction Into and Out of Levels

Pt^{192}

Level	In	Out	Difference
H	-	0.5	0.5
G	-	8	8
F	-	-	-
E	-	44	44
D	2	54	52
C	38	39	1
B	98	89	-9
A	96	-	

Os^{192}

E	-	1.6	1.6
D	1.6	3.8	2.2
C	$(0.5)^{*}(4.1)^{**}$	$(0.5)^{*}(3.8)^{**}$	-
B	$(3.8)^{*}(0.5)^{**}$	$(4.1)^{*}(0.5)^{**}$	-
A	4.1		

* for schemes 10 a and b

** for scheme 10 c

well with the measurement of 1490 ± 20 kev, made by Pringle, et al (42).*

The calculated values of log ft for the four beta transitions are:

Trans. to Level	Beta Energy	log ft
D	673 ± 10 kev	8.3
E	536 ± 10 kev	8.1
G	256 ± 10 kev	8.1
H	99 ± 12 kev	> 8.1

These values of log ft are associated with first forbidden beta transitions (43). The selection rules for first forbidden transitions are that the parity changes, and the spin changes by 2 or less ($\Delta I = 0, \pm 1, \pm 2$; yes). In addition, Nordheim has suggested some composition rules, one of whose consequences is that spin changes of ±1 are excluded, (43).

ii. Os^{192} **

The decay fractions indicate that ~3.5% of the Ir^{192} decays go by electron capture to Os^{192}. The electron capture transitions go to levels D and E, with the relative intensities 2:1.5. The possibility of transitions to the ground state cannot be eliminated, although because of the spin change (see part H) no such transitions are expected. No positron spectrum has been detected, and an upper limit of 10^{-6} positrons/decay can be put on the intensity of positron emission. From the known energy dependence of the ratio of positron emission to K-capture (44), one can put an upper limit of 1.3 Mev on the energy of the transition to level D.

---

* The method employed for the measurement of the Ir^{192} - Pt^{192} mass difference was to immerse a powdered source of Ir^{192} in a liquid scintillator, and observe the end point of the beta- plus gamma-ray pulse height spectrum.

** The discussion in this section applies equally to all three of the proposed energy level schemes (fig. 10).

This puts an upper limit of 2 Mev on the Ir^{192} - Os^{192} mass difference.

If the mass difference were known, the log ft values for the electron capture transitions could be calculated. On the other hand, if the log ft values were known, the mass difference could be calculated. If it is assumed that the log ft value for electron capture should not differ greatly from the values in the competing beta emission, that is, if log ft = 8.2 ± 1.0, the calculated mass difference is 1.2 ± 0.5 Mev.

H. Spins and parities

i. Pt^{192}

Pt^{192} is an even-even nucleus, and it is assumed that the spin and parity of its ground state is 0+. Levels B and C both decay by E2 transitions to the ground state - consequently the spins and parities of both levels must be 2+.

The spin of level D was determined by the angular correlation of the 316 and 467 kev gamma rays. Both transitions are E2. Since the spin of level B is 2, and B is reached by E2 transition from level D, the spin of level D must lie between 0 and 4. Its parity is the same as that of level B.

Fig. 14 shows the theoretical angular correlation functions for two quadrupole transitions between levels of spins J - 2 - 0, where J takes on the values 0 to 4. The curves have been corrected for the size of the detectors by the method of Rose (24). (The source to detector distance was 5 cm - the correction coefficients have been given in section III. D). The experimental points are shown on the same graph. The standard deviation, which has been indicated only for the point at $\theta = 135^{\circ}$, is the same for all observations. The experimental points

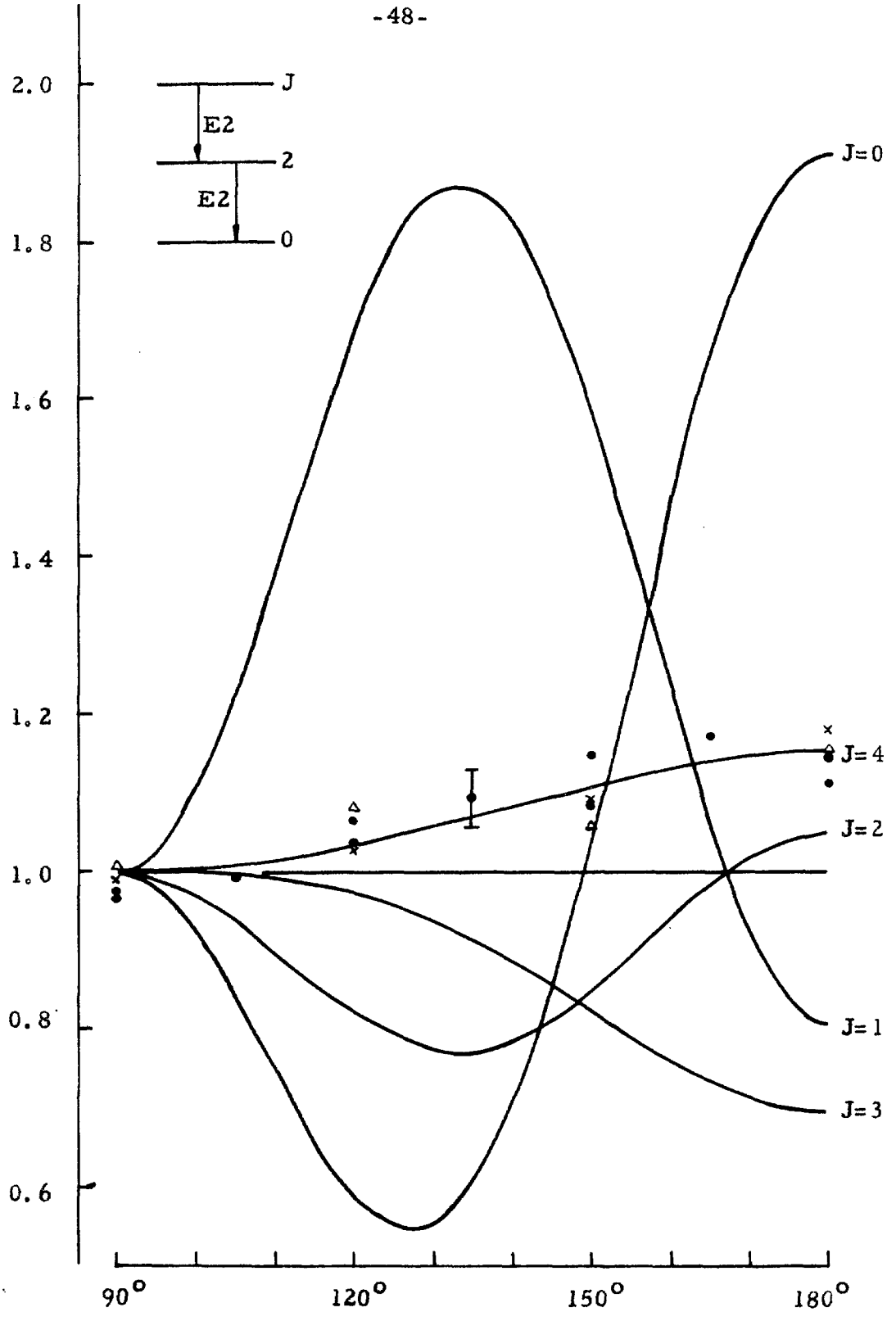

Fig. 14. Angular correlation of the 316 and 467 kev gamma rays. The curves are the theoretical correlation functions for two quadrupole transitions between states having spins J, 2, 0. They have been corrected for the size of the detectors. Three sources were used, indicated by the marks ● (metallic Ir evaporated on mica), X ($IrCl_3$ dissolved in HCl), △($IrCl_6^{=}$ complex in a precipitate).

clearly fit best with the curve for J = 4, and this is the spin assigned to level D.

The spin of level G was determined by the angular correlation between the 588 and 613 kev lines. The analysis is similar to that above. Both transitions are E2, connecting levels of spins J - 2 - 0. The theoretical angular correlation curves for the various possible values of J are shown in fig. 15, along with the experimental points. (The source to detector distance in this case was 3 cm - which is responsible for the difference between the theoretical curves and those of fig. 14). Again, the best fit is with the curve for J = 4.

The experimental evidence for the other spins is more indirect. As will be shown in the next part, the spin of the Ir^{192} ground state must be 5 or 6, with odd parity. The beta transition to level E is first forbidden - hence, the spin of level E cannot be lower than 3. Strong E2 transitions connect this level with levels B and C, both of which have spin 2. Therefore, the spin of level E cannot be greater than 4. Its assignment, then, is (3 or 4)+.

Beta transition to level F (if the level exists) is at least second forbidden (log ft > 10.5). The spin of this level, therefore, must be less than 4. Since the major evidence for the existence of this level is a transition to the ground state, the spin should be less than 3. Gamma transitions are strictly forbidden for 0 - 0 transitions, so spin 0 is excluded. One is left with the possibilities 1 and 2 for the spin of level F. Its parity cannot be assigned.

That some weak transitions from level H have been observed indicates that a beta transition to this level is probably no more than first forbidden. That the transitions are weak indicates that it is not

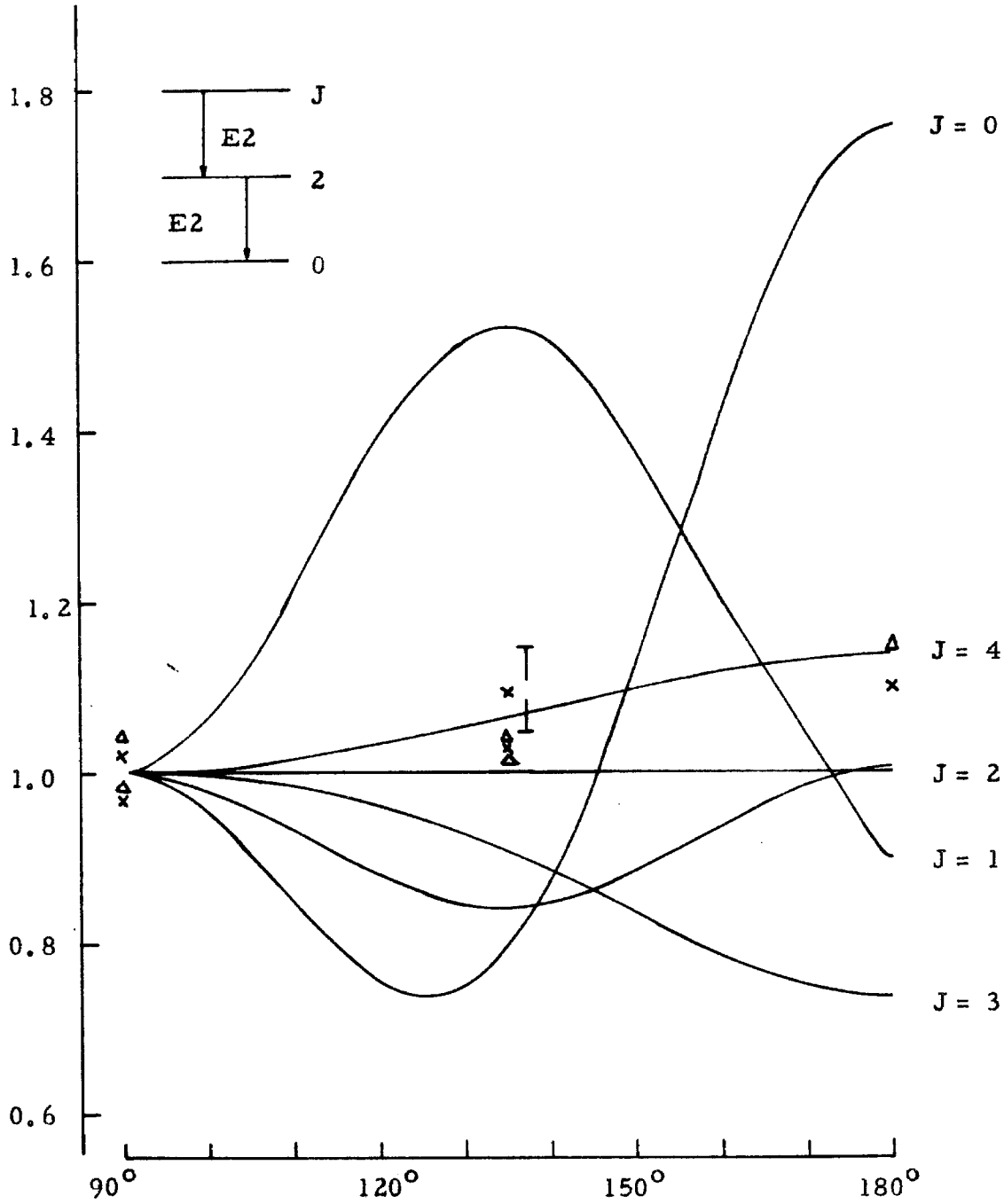

Fig. 15. Angular correlation of the 588 and 612 kev gamma rays. The curves are the theoretical correlation functions for two quadrupole transitions between states having spins J, 2, 0. They have been corrected for the size of the detectors. Two sources were used, indicated by the marks X ($IrCl_3$ dissolved in HCl) and Δ ($IrCl_6^{=}$ complex in a precipitate).

allowed. The gamma ray to level C (spin 2) limits the spin of level H to 4 or below. We have, therefore, assigned its spin as (3 or 4), with even parity.

ii. Ir^{192}

We have noted that the beta transitions to the 4+ levels, D and G, are first forbidden transitions ($\Delta I = 0, (\pm 1), \pm 2$; yes). The Ir^{192} nucleus, then, must have a spin between 2 and 6, and odd parity. If its spin were 2, 3 or 4, transitions to levels B and C (which are 2+ levels) would also be first forbidden, and one would expect to see reasonably strong transitions to these levels. The absence of such transitions indicates that the spin of the Ir^{192} nucleus must be greater than 4. Nordheim's compositions rules (42) (which exclude the spin change $\Delta I = \pm 1$) lend weight to the choice of a 6- assignment for the Ir^{192} nucleus. However, this does not seem strong enough to eliminate completely the possibility of a 5- assignment.

iii. Os^{192}

The ground state spin of Os^{192} is assumed to be 0, and its parity even. Level B decays by an E2 transition to the ground state, and so must be a 2+ state.

Level D is substantially fed by electron capture transitions. On the basis of the previously argued spin of the Ir^{192} nucleus, the spin of level D cannot be less than 3. Because of the E2 transition to level B (spin 2), level D's spin cannot be greater than 4. The assignment, therefore, is (3 or 4)+.

In the scheme of fig. 10 c, level C decays to the ground state by an E2 transition, so its assignment is 2+. In the schemes of figs. 10 a and b, the crossover transition from C to A has not been observed.

Level C appears to have no feeding by electron capture. Its spin, therefore, must be less than 4. The E2 transition from level D requires that its spin be at least 1. The assignment is (1, 2 or 3)+.

The arguments for the spin of level E are contrary. There seems to be a relatively strong electron capture transition to this level - hence its spin should not be lower than 3. However, there is a gamma transition to the ground state (spin 0), and none to levels B or C. This clearly indicates a spin of 2 or less. No assignment was made.

I. General

It is of interest to see how the assignment of 5- or 6- for the spin and parity of the ground state of Ir^{192} can be interpreted on the basis of the shell model. Ir^{192} has 77 protons and 115 neutrons. According to the compilation by Klinkenburg (45), the 77th proton in Ir^{191} and in Ir^{193} is in a d(3/2) orbit. Recent investigations by Mihelich, McKeown and Goldhaber (46)(47) indicate that the ground state of Os^{191} (115 neutrons) must have spin and parity 9/2 -. If a single-particle description is applicable to this case, this would indicate an h (9/2) orbit for the odd neutron. This seems a bit surprising. According to Klinkenberg's tables, the configurations of the neighboring odd-neutron nuclei are

N	Nucleus	Neutron config.	Ground state
109	W^{183}	$(i\ 13/2)^2\ (p\ 1/2)$	p(1/2)
111	Os^{187}	$(i\ 13/2)^4\ (p\ 1/2)$	p(1/2)
113	Os^{189}	$(i\ 13/2)^6\ (p\ 1/2)$	p(1/2)
117	Pt^{195}	$(i\ 13/2)^{10}(p\ 1/2)$	p(1/2)
119	Hg^{199}	$(i\ 13/2)^{12}(p\ 1/2)$	p(1/2)

This indicates that the i(13/2) shell is filling pairwise, with the odd neutron found in a p(1/2) shell. It may be that the neutron configuration with 115 neutrons must be described by a mixture of single-particle configurations.

The 3/2 spin of the proton can couple with the 9/2 neutron spin to give a spin between 3 and 6. Nordheim has suggested as a "composition rule" for odd-odd nuclei that if the two odd nucleons are in the same Schmidt group ($j_P = l_P + \frac{1}{2}$, $j_N = l_N + \frac{1}{2}$; or $j_P = l_P - \frac{1}{2}$, $j_N = l_N - \frac{1}{2}$), the resultant spin will be larger than the minimum. This rule is consistent with the assigned spin of Ir^{192}.

With respect to the regularities of the spectra of heavy even-even nuclei, described in the Introduction (sect. II), we find the following:

Energies of the first excited states of Pt^{192} and Os^{192} fit quite well with those of the neighboring nuclei (see fig. 1).

The E_2/E_1 ratio in Pt^{192} is 1.94, which fits well with the ratios of the other Pt isotopes (fig. 2). The E_2/E_1 ratio in Os^{192} is 1.98, 2.38 or 2.41 for the energy level schemes 10 a, b or c.

The sequence of spins and parities of the first three states of Pt^{192} is 0+, 2+, 2+. The sequence in Os^{192}, for level schemes 10 a and b, is 0+, 2+, (1, 2 or 3)+, while for level scheme 10 c, the sequence is 0+, 2+, 2+.

Two intensity rules have been suggested by Scharff-Goldhaber and Weneser (5), which seem to govern the electromagnetic transitions in those even-even nuclei having a 2+ second excited state. The rules are: a) between the second and first 2+ state, the transition is usually mainly E2, with only a small admixture of M1; b) the probability of the E2 part of the second-to-first excited state transition relative to that of the

competing crossover transition is much larger than would be expected on the basis of the single particle model (that is, on the basis of Weisskopf's lifetime formula, (48)).

These intensity rules, which were deduced from the study of the medium weight even-even nuclei, seem also to apply to the decays reported here. The transition from the second-to-first excited state in Pt^{192} (296 kev) has less than 5% M1 admixture. The crossover transition from level C to A is relatively weak. The ratio of the reduced transition probabilities* of the 295 and 612 kev transitions is 163:1.

The second-to-first excited state transition in Os^{192} is also mostly E2. The 201 kev transition (scheme 10a) appears to have ~20% M1 admixture; the 283 kev transition (schemes 10 b and c) has less than 10% M1 admixture. The crossover is not observed in schemes 10 a and b. If the crossover were as intense as the 201 or 283 kev transitions it would certainly have been observed. On this basis, the ratio of the reduced transition probabilities of the 201 and the (unobserved) 407 kev transitions (scheme 10 a) is $> 32:1$; the ratio for the 283 and the (unobserved) 489 kev transitions is $>15:1$. In scheme 10 c, the crossover is fairly strong. The ratio of reduced transition probabilities of the 283 and 484 kev transitions is 2.5:1.

---

* The reduced transition probability for a transition of multipole order L and energy ΔE is proportional to the transition probability divided by $(\Delta E)^{2L+1}$ (see ref. 6, p. 101).

Appendix I

Relative intensities of the gamma rays of Ir^{192}, measured by gamma spectrometer (see sect. IIIA, part iv).

Energy	Uncorrected Intensity	mult. by Self Absorption	mult. by Detector Efficiency
136.3	8.2	2.5	1.00
201.3	11.2	1.50	1.03_5
205.7	95	1.46	1.04
283.3	6.5	1.21	1.14
295.9	390	1.19	1.17
308.4	375	1.17_5	1.19
316.4	1000	1.16	1.21
374.7	19	1.11	1.37
468.0	206	1.07_5	1.70
484.7	10	1.07_5	1.76
588.4	6.9	1.05_5	2.10
604.5	18	1.05	2.13
612.9	13	1.05	2.15

Appendix II

Separation of Iridium (see sect. III B, part iii) from W. W. Meinke, UCRL-432, Aug. 30, 1949.

Time for separation: 1 hour

Equipment: small porcelain crucible
transfer pipettes
centrifuge tubes

Yield: ~50% (depending on step 3)

Degree of purification: At least factor of 100.

A simple, reasonably fast procedure for solution and separation with a target material (Ir) extremely resistant to dissolution in aqua regia.

Procedure:

(1) Make a melt of KOH and KNO_3 (approx. 50-50, not critical) in a small porcelain crucible, heating strongly over a Fischer burner.

(2) To this hot flux add the target Ir metal, continuing to heat (and adding KOH if volume of flux gets too small) until the metal is completely dissolved. (For a small strip of 1 mil foil this should take no longer than 5-10 min.)

(3) Allow flux to cool, then leach for ~5 min. with conc HCl, adding Au and Pt carriers in small amount. (Ir gives strong blue colored sol'n.)

(4) Extract twice with ethyl acetate to remove Au.

(5) Add a little $SnCl_2$ solution in HCl to the aqueous phase until a dark red coloration (H_2PtCl_4) indicates the reduction of Pt from +4 to +2 state is complete. (See remarks.)

(6) Extract the red coloration (Pt) into ethyl acetate. Wash organic layer twice with equal volume of 3N HCl. After complete removal of Au and Pt, Ir can be extracted as follows:

(7) Reoxidize the aqueous phase from above by addition of a small amount of 30% H_2O_2. (Reappearance of blue Ir^{VI} coloration.)

(8) Add a little NH_4SCN solution. (Blue changes to beautiful pink.) A precipitate of $(Ir)_x(SCN)_y$ forms slowly. (The rate of precipitation is slow enough that one may make use of the fact that the pink compound is extractable into ethyl acetate.)

The extraction of the pink compound has the advantage of quickly removing the Ir from the original solution, which usually has enough silica dissolved (from crucible) that the whole solution will gel if allowed to stand.

The pink compound precipitates from the ethyl acetate on standing.

Remarks:

As most Ir foil contains about 1% Pt impurity, it is well to provide a step for extraction of Au activities, whether or not the Au is desired for later work, even if it is simply a proton bombarded Ir foil.

On $SnCl_2$ reduction the strong blue coloration of Ir(+6?) disappears, permitting the red of reduced H_2PtCl_4 to be seen.

By spending more time leaching the melt (3) and by using several portions of leaching agent the chemical yields might be made almost quantitative.

References

(1) J. M. Hollander, I. Perlman and G. T. Seaborg: Rev. Mod. Phys., 25, 469 (1953).

(2) P. Stähelin and P. Preiswerk: Helv. Phys. Acta, 24, 623 (1951); Nuovo Cimento, 10, 1219, (1953).

(3) P. Preiswerk and P. Stähelin: Physica, 18, 1118 (1952).

(4) G. Scharff-Goldhaber: Physica, 18, 1105 (1952); Phys. Rev., 90, 587 (1953).

(5) G. Scharff-Goldhaber and J. Weneser: Phys. Rev., 98, 212, (1955).

(6) A. Bohr and B. Mottelson: Kgl. Danske Vids. Selsk, Mat.-Fys. Medd., 27, no. 16 (1953).

(7) A. Bohr: "Rotational States of Atomic Nuclei," (thesis) Ejnar Munksgaard, Copenhagen, 1954.

(8) A. Bohr and B. Mottelson: Chapter 17, Beta- and Gamma-Ray Spectroscopy, edited by K. Siegbahn, North-Holland Publishing Company, Amsterdam, 1955.

(9) J. W. M. DuMond: Rev. Sci. Inst., 1, 2 (1930); 18, 626 (1947).

(10) J. W. M. DuMond: Chapter 4, Beta- and Gamma-Ray Spectroscopy, edited by K. Siegbahn, North-Holland Publishing Company, Amsterdam, 1955.

(11) J. W. M. DuMond: Erg. d. Exact. Naturwiss., 28, 232 (1955).

(12) D. A. Lind, thesis, California Institute of Technology (1948).

(13) P. Marmier: private communication

(14) D. A. Lind, W. J. West and J. W. M. DuMond: Phys. Rev., 77, 475 (1950).

(15) J. W. M. DuMond: Rev. Sci. Inst., 20, 160 (1949).

(16) J. W. M. DuMond, J. Kohl, L. Bogart, D. E. Muller and J. R. Wilts, Office of Naval Research Special Technical Report No. 16, March 1952 (unpublished).

(17) J. J. Murray, thesis, California Institute of Technology (1954).

(18) W. W. Meinke, "Chemical Procedure Used in Bombardment Work at Berkeley," University of California Radiation Laboratory Report, UCRL-432, August 30, 1949 (unpublished).

(19) W. C. Elmore and M. Sands: Electronics, Experimental Techniques, McGraw-Hill, New York, 1949.

(20) D. Maeder, R. Müller and V. Wintersteiger: Helv. Phys. Acta, 27, 3 (1954).

(21) J. W. Dunworth: Rev. Sci. Inst., 11, 167 (1940).

(22) E. L. Brady and M. Deutsch: Phys. Rev. 72, 870 (1947).

(23) L. C. Biedenharn and M. E. Rose: Rev. Mod. Phys., 25, 729 (1953).

(24) M. E. Rose: Phys. Rev., 91, 610 (1953).

(25) H. Frauenfelder: Chapter 19, Beta- and Gamma-Ray Spectroscopy, edited by K. Siegbahn, North-Holland Publishing Company, Amsterdam, 1955.

(26) Fermi, Amaldi, D'Agostino, Rasetti and Segre: Proc. Roy. Soc. London, 146A, 483 (1934).

(27) E. Amaldi and E. Fermi: Ricerca Scientifica, 7, 56 (1936).

(28) L. J. Goodman and M. L. Pool: Phys. Rev. 71, 288 (1947).

(29) J. Kastner: Can. J. Phys., 29, 480 (1951).

(30) W. Rall: Phys. Rev., 70, 112 (1946).

(31) J. M. Cork, J. M. LeBlanc, A. E. Stoddard, W. J. Childs, C. E. Branyan and D. W. Martin: Phys. Rev., 82, 258 (1951).

(32) M. W. Johns and S. V. Nablo: Phys. Rev., 96, 1599 (1954).

(33) G. T. Ewan and A. L. Thompson: Trans. Roy. Soc. Can. 47, 126 (1953) also quoted in (32).

(34) M. E. Rose: Chapter 14, Beta- and Gamma-Ray Spectroscopy, edited by K. Siegbahn, North-Holland Publishing Company, Amsterdam, 1955.

(35) D. Lu and M. Wiedenbeck: Phys. Rev., 94, 501 (1954).

(36) N. P. Heydenburg and G. M. Temmer: Phys. Rev., 93, 906 (1954).

(37) N. P. Heydenburg: private communication.

(38) R. A. Naumann: Phys. Rev., 96, 90 (1954).

(39) G. J. Nijgh, L. T. M. Ornstein, N. Grabben, and A. H. Wapstra: Proceedings of the 1954 Glasgow Conference on Nuclear and Meson Physics, Pergamon Press, London and New York, p. 229, 1955.

(40) P. W. Levy: Phys. Rev., 72, 352 (1947).

(41) V. S. Spinel and N. V. Forafontov: Zhur. Eksptl. i Teor. Fiz., 21, 1376 (1951).

(42) R. W. Pringle, W. Turchinetz and H. W. Taylor: Phys. Rev., 95, 115 (1954).

(43) L. W. Nordheim: Rev. Mod. Phys., 23, 322 (1951).

(44) E. Feenberg and G. Trigg: Rev. Mod. Phys., 22, 399 (1950).

(45) P. F. A. Klinkenberg: Rev. Mod. Phys., 24, 63 (1952).

(46) J. W. Mihelich, M. McKeown and M. Goldhaber: Phys. Rev., 96, 1450 (1954).

(47) J. W. Mihelich, M. Goldhaber: Bull. Amer. Phys. Soc., 30, No. 1, Abstract S1 (1954).

(48) J. M. Blatt and V. F. Weisskopf: Theoretical Nuclear Physics, John Wiley, New York, p. 595, 1952.